Dietary potassium restriction causes hypercalciuria, hypocalcemia and bone loss in male mice

Sathish K Murali[1*], Mariavittoria D'Acierno[2*], Xiang Zheng[2], Lena K Rosenbaek[2], Louise N. Odgaard[2], Richard Grimm[3], Alice Ramesova[1], Robert Little[2,4], Judith Radloff[1], Paul A. Welling[3], Qi Wu[2], Reinhold G Erben[5], and Robert A Fenton[2]

* Equal contribution

[1] Department of Biomedical Sciences, University of Veterinary Medicine, Vienna, Austria

[2] Department of Biomedicine, Aarhus University, Aarhus, Denmark

[3] Department of Medicine, Division of Nephrology, Johns Hopkins University School of Medicine, Baltimore, MD, USA.

[4] Institute of Neuroscience and Cardiovascular Research, University of Edinburgh, Edinburgh, UK

[4] Ludwig Boltzmann Institute of Osteology, Vienna, Austria

Running title: Dietary potassium and bone

Key words: NCC, calcium homeostasis, 1,25(OH)2D, calcitropic, phosphaturic

Conflict of interest. The authors have declared that no conflict of interest exists.

Word Count: 11,185 (all sections including references and figure legends)

Correspondence: Robert A. Fenton, Aarhus University, Department of Biomedicine, Hoeegh-Guldbergs Gade 10, Building 1115, DK-8000 Aarhus C, Denmark. E-mail: Robert.a.fenton@biomed.au.dk, phone: 004587167671

Abstract

Loss of bone mass has a devastating effect on quality of life. Higher potassium (K^+) intake is positively correlated with bone health. Here, we investigated whether kidney calcium (Ca^{2+}) and phosphate (Pi) handling mechanisms mediate dietary K^+ effects. Kidney Ca^{2+} and Pi handling proteins were altered in abundance in mice fed a 0% K^+ diet for 2 weeks. In mice fed a 0.1% K^+ diet for 4 or 8 weeks, urinary Ca^{2+} excretion increased, plasma Ca^{2+} levels were lower and plasma parathyroid hormone (PTH) levels were higher relative to control 1% K^+ fed mice. The 0.1% K^+ fed mice had greater excretion of the bone resorption marker deoxypyridinoline, increased osteoclast number, and decreased total femoral bone mineral density. During chronic low K^+ intake, major changes in renal Ca^{2+} and Pi transport pathways were absent, except higher abundances of the sodium-potassium-chloride co-transporter (NKCC2) and the sodium-chloride co-transporter (NCC), in line with their role in kidney Ca^{2+} handling. Low dietary K^+ induced hypocalcemia and changes in PTH were absent in mice with constitutively active NCC, supporting its role in mediating low K^+ effects on Ca^{2+} homeostasis. Our study provides insights into the management of bone disorders in conditions of chronic electrolyte imbalance.

Introduction

Calcium (Ca^{2+}) and phosphate (Pi) homeostasis is critical for numerous physiological processes, especially in maintaining skeletal integrity. Ca^{2+} is the most abundant mineral in the human body and controlling Ca^{2+} homeostasis is essential for bone mineralization, nerve transmission, hormone secretion, muscle contraction, and blood clotting (1). Similarly, Pi plays vital roles in bone formation, as well as cellular energy metabolism and signaling. As well as being integral components of bone hydroxyapatite, plasma Ca^{2+} and Pi levels modulate the activity of bone forming osteoblasts, and bone-resorbing osteoclasts, thereby playing major indirect roles in bone turnover (2).

Ca^{2+} and Pi homeostasis is maintained by integrated uptake, storage and excretion by the intestine, bone and kidney (3, 4), controlled by the actions of parathyroid hormone (PTH), 1,25-dihydroxy-Vitamin D_3 (1,25(OH)2D; active vitamin D or calcitrol), fibroblast growth factor 23 (FGF23) and its co-receptor Klotho (3, 4). In addition, the calcium-sensing receptor (CaSR), which senses changes in extracellular Ca^{2+} to modulate cellular signaling, plays a multifaceted role in Pi and Ca^{2+} homeostasis by modulating release of PTH and by directly altering renal Ca^{2+} handling (5-7). In the kidney, the effects of PTH and 1,25(OH)2D are mediated through alterations in Ca^{2+} and Pi transport across the renal tubule. Renal reabsorption of Pi occurs exclusively in the proximal tubules (PT) via the sodium-dependent Pi transporters NaPi-2a and NaPi-2c, as highlighted by the hypophosphatemia, hyperphosphaturia and bone defects of NaPi-2a deficient mice (8). PTH can reduce apical membrane NaPi-2a abundance and increase urinary excretion of Pi (9). FGF23, a hormone produced primarily by osteocytes and osteoblasts, also acts as a phosphaturic factor and increases renal Pi excretion by reducing NaPi-2a and NaPi-2c levels (10), whereas 1,25(OH)2D signaling via the vitamin D receptor (VDR) increases kidney Pi reabsorption (11).

The majority (60-70%) of renal Ca^{2+} reabsorption occurs paracellularly in the PT, driven by active transcellular Na^+ transport via the Na^+/H^+ exchanger isoform 3 (NHE3) (12, 13). In line with this, total NHE3 knockout mice have urinary Ca^{2+} wasting and reduced bone mass (14), but paradoxically PTH

stimulates kidney Ca^{2+} reabsorption whilst inhibiting NHE3 activity (6). In addition to the PT, approximately 20% of Ca^{2+} reabsorption occurs paracellularly in the thick ascending limb (TAL), driven by the luminal positive voltage generated by the Na-K-2Cl co-transporter (NKCC2) (15-17), which is activated by PTH (1). Finally, the distal convoluted tubule (DCT) and the connecting tubule reabsorb approximately 10% of filtered Ca^{2+} via the transient receptor potential cation channel subfamily V member 5 (TRPV5) (18). FGF23 and PTH can increase TRPV5 activity (19, 20) and are associated with higher distal tubule Ca^{2+} transport (21), and renal Ca^{2+} reabsorption in the DCT/CNT can partially compensate for the reduced PT Ca^{2+} transport in mice with kidney-specific NHE3 deletion (22), suggesting an underappreciated role of this segment in overall Ca^{2+} homeostasis.

There is emerging evidence that potassium (K^+) may influence Ca^{2+} and Pi homeostasis, with a positive relationship between dietary K^+ intake and bone health (23-25). For example, administration of K^+ (K^+-citrate) in postmenopausal women with osteopenia was proposed to reduce the body's acid load, subsequently improving bone mineral density (BMD) (26). A positive effect of K^+ supplementation on BMD was also reported in healthy older adults without osteoporosis (27), which was again linked to alterations in acid-base balance. However, K^+ supplementation can also alter kidney Ca^{2+} and Pi handling, which may influence bone formation and resorption rates and overall bone health independent of acid-base effects (28). For example, in pre-hypertensive individuals, K^+ supplementation increases plasma Pi and decreases renal Ca^{2+} excretion, effects that are independent of the anion accompanying the K^+ (29, 30). Furthermore, alterations in extracellular fluid (ECF) K^+ concentrations subsequent to changes in dietary K^+ intake modulates activity of the NaCl cotransporter NCC in the DCT, which can indirectly alter Ca^{2+} reabsorption via TRPV5 (31-33). The importance of this mechanism is highlighted by the Ca^{2+} balance defects observed in patients with Gitelman syndrome or Familial Hyperkalemia with Hypertension (FHHt)) (34-36) and altered NCC activity. Furthermore, pharmacological NCC inhibition with thiazides reduces urinary Ca^{2+} excretion and has been associated with higher BMD and lower fracture risk in several cohorts, although there are context-specific effects (37, 38).

The average dietary K^+ intake (70 mmol/day) for adults is much lower than the recommended intake, likely a result of ultra-processed diets that are low in K^+ and our reduced consumption of fruit and vegetables (32). The consequences of low dietary K^+ on blood pressure and the risk of cardiovascular disease are well established (39). However, although associations between increased dietary K^+ intake and improved bone health exist, the consequences of a low dietary K^+ intake on bone metabolism are less clear. Therefore, the aim of this study was to investigate in male mice the effects of chronic low dietary K^+ intake on Ca^{2+} and Pi homeostasis, bone metabolism and the potential molecular mechanisms underlying any effects. The major finding from our study is that low dietary K^+ intake causes hypercalciuria, hypocalcemia, higher plasma PTH, and decreased BMD. We propose that the molecular basis of these effects involves reduced distal tubule Ca^{2+} reabsorption subsequent to increased NCC activity.

Results

A K^+ deficient diet for two weeks alters numerous proteins associated with kidney Ca^{2+} and Pi handling. In study 1, mice were fed a control diet containing 1% K^+ (referred to as $1K^+$) or a diet deficient in K^+ (referred to as $0K^+$) for 2 weeks (Figure 1A). Average 24 h food intake was not significantly different between the groups (Supplemental Figure 1). Relative to $1K^+$ fed mice, $0K^+$ fed mice had significantly lower plasma K^+ and plasma total Ca^{2+} concentrations, whereas plasma PTH levels were ~2-fold higher (Figure 1B). Plasma 1,25(OH)2D (calcitriol) concentrations were significantly higher in $0K^+$ fed mice (Figure 1B), in line with higher *Cyp27b1* mRNA levels (Supplemental Table S1). Fractional excretion (FEx) of K^+ and Cl^- were significantly lower, whereas FEx of Ca^{2+} and Pi were higher (Figure 1C, daily excretions shown in Supplemental Figure 2). Urine aldosterone levels were greatly reduced in mice fed a $0K^+$ diet (Figure 1C). To investigate the broad effects of a $0K^+$ diet on the protein landscape of the kidney and to identify in an unbiased manner how dietary K^+ may influence Ca^{2+} and Pi homeostasis, we analyzed kidney protein abundances using liquid chromatography–tandem mass spectrometry–based (LC-MS/MS–based) quantitative proteomics. All quantified proteins, their relative abundances and their general classification are found in Supplemental Data 1. Of the 6078 proteins that were quantified, 333 were significantly reduced and 773 significantly increased in abundance after the $0K^+$ diet relative to the $1K^+$ diet-fed mice (Figure 1D). Several of the significantly changed proteins are directly or indirectly associated with Ca^{2+} and/or Pi homeostasis. These included reduced abundances of klotho, the Na^+/H^+ exchanger isoform 3 (NHE3, *Slc9a3*) sodium/calcium exchanger 1 (NCX1, *Slc8a1*), the sodium-potassium-chloride cotransporter NKCC2, the sodium-dependent phosphate transport protein 2A (Napi2a, *Slc34a1*), the NHE3 and Napi2a scaffolding protein NHERF3 (*Pdzk1*), the Ca^{2+} binding proteins Calbindin28K (*Calb1*) and parvalbumin (*Pvalb*), the plasma membrane calcium-transporting ATPase 4 (PMCA4, *Atp2b4*), and the paracellular claudin-8 (*Cldn8*). Increased abundances of claudin-3 (*Cldn3*), uromodulin (*Umod*), the Ca^{2+} transporter TMEM165 (*Tmem165a*) and osteopontin (*Spp1*) were detected (Figure 1D). Several of the observed changes at the protein level were also detectable at the mRNA level (Supplemental Table S1). Gene

ontology (GO) and Ingenuity Pathway Analysis (IPA) further supported a general alteration in Ca^{2+} and Pi transport pathways, or Ca^{2+} mediated signaling pathways in the kidney during dietary K^+ deficiency (Supplemental Data 1 and Figure 1E). An increase in Rho and Rac signaling pathways during K^+ deficiency is in line with hypertrophy of proximal tubule cells and increased density and length of microvilli (40), which could also influence Na^+ and hence Ca^{2+} transport. Furthermore, IPA highlighted that several of the proteins that were significantly altered in abundance after $0K^+$ feeding are linked to various nephrotoxicity pathways or are associated to kidney damage (Supplemental Figure 3), in line with what we have observed previously with extreme alterations in dietary K^+ intake (41).

Long-term low dietary K^+ intake results in increased urinary Ca^{2+} excretion, hypocalcemia, and higher plasma PTH levels. In study 2, our aim was to assess the consequences of a prolonged reduction in dietary K^+ intake on Ca^{2+} and Pi homeostasis. Therefore, rather than feeding mice a diet completely deficient in K^+, mice were provided diets containing either 0.1% K^+ (referred to as $0.1K^+$) or 1% K^+ (referred to as $1K^+$) for 4 or 8 weeks (Figure 2A). Average food intakes measured in home cages over the duration of the study were not significantly different between the groups (4 weeks $1K^+ = 0.16 \pm 0.01$ vs $0.1K^+ = 0.18 \pm 0.03$; 8 weeks $1K^+ = 0.14 \pm 0.02$ vs $0.1K^+ = 0.15 \pm 0.01$; g food / g BW / day, mean ± SD). Bodyweight changes between the groups or timepoints were not significantly different (Supplemental Figure 4). At both the 4 week and 8 week points, mice fed the $0.1K^+$ diet had significantly lower plasma K^+ levels (Figure 2B) and urinary FEx K^+ (Figure 2C and Supplemental Figure 2). Plasma total Ca^{2+} levels were significantly lower in mice fed the $0.1K^+$ diet (Figure 2B), whereas FEx Ca^{2+} and daily urinary Ca^{2+} excretion were significantly higher (Figure 2C and Supplemental Figure 2). Plasma Pi levels were significantly higher in mice fed a $0.1K^+$ diet after 8 weeks, consistent with a significantly lower urinary Pi excretion and FEx Pi at this time point (Figure 2, B and C and Supplemental Figure 2). Plasma concentrations and daily urinary excretions of Na^+ and Cl^- were not significantly different between the groups at both 4 and 8 weeks (Figure 2, B and C). In line with the dietary K^+ restriction, urinary aldosterone excretion was significantly lower in $0.1K^+$ fed mice compared to the $1K^+$ control group (Figure 2C). Long-term dietary K^+ restriction led to a

significant increase in plasma PTH levels, but unlike study 1 ($0K^+$ diet), the levels of 1,25(OH)2D were not significantly different (Figure 2D), nor were *Cyp27b1* mRNA levels (Supplementary Table S2*)* or plasma FGF23 concentrations (Figure 2D). In mice on the $0.1K^+$ diet, the mRNA expression of the CaSR was increased at both timepoints (Table 1), whereas expression of *Fgfr1* (encoding the Fgf receptor 1) and the *Pth1r* (encoding the PTH receptor) were only increased at the 4-week stage (Supplementary Table S2).

Prolonged dietary K^+ restriction decreases femoral midshaft total bone mineral density (BMD). Lower levels of plasma Ca^{2+} results in secondary hyperparathyroidism, subsequently followed by disturbances in bone turnover, decreased BMD and reduced bone integrity (42, 43). The hypocalcemia together with elevated plasma PTH suggests that a similar impairment of bone integrity may occur during dietary K^+ depletion. To examine this, BMD was assessed using peripheral quantitative computed tomography (pQCT) in femoral bones isolated from mice fed $0.1K^+$ or $1K^+$ diets for 4 or 8 weeks. At the metaphysis, periosteal and endosteal perimeter were comparable between mice on different K^+ intakes (Figure 3A), indicating no significant changes in metaphysis bone geometry. However, trabecular BMD was significantly reduced in the $0.1K^+$ fed group at both time points, and total BMD was significantly lower after 8 weeks, indicating progressive loss of trabecular bone with prolonged K^+ deficiency (Figure 3A). At the midshaft, total BMD was significantly lower in mice receiving a $0.1K^+$ diet compared to $1K^+$ controls (Figure 3, B and C). Despite this reduction in total BMD, cortical BMD and cortical thickness were similar between the groups, indicating that the cortical bone compartment was not markedly affected by K^+ depletion. Interestingly, while periosteal and endosteal circumference were comparable between the groups after 4 weeks, both parameters were significantly increased in the $0.1K^+$ fed group after 8 weeks, suggesting cortical expansion at the femoral midshaft (Figure 3, B and C). To analyze microarchitecture in trabecular and cortical bone we used micro-CT. After 4 weeks of the two dietary regimes, no significant changes at the femoral metaphysis in trabecular number, thickness, and spacing were detectable (Figure 3D). However, after 8 weeks, mice receiving the $0.1K^+$ diet had significantly lower trabecular number and trabecular BMD, with significantly greater trabecular spacing (Figure 3D). In the midshaft region, micro-CT analysis

confirmed the findings from pQCT, with total BMD significantly reduced in the $0.1K^+$ diet group with no detectable changes in cortical BMD or cortical thickness (Figure 3E). Together these results suggest that prolonged dietary K^+ depletion selectively impacts trabecular bone architecture and total BMD while having minimal effects on cortical bone mass.

Low dietary K^+ intake increases bone osteoclast activity. Hyperparathyroidism promotes bone resorption (44, 45). To further investigate the effects of low dietary K^+ intake on bone remodeling and mineralization, we performed histomorphometric analyses of longitudinal femur sections using TRAP (tartrate-resistant acid phosphatase) staining for bone resorption, von Kossa/McNeal staining for bone mineralization and double calcein labeling for bone formation. After 4 and 8 weeks, there was a significant increase in osteoclast surface and osteoclast number in femurs from mice receiving $0.1K^+$ diets relative to $1K^+$ control diets (Figure 4A) and urinary excretion of deoxypyridinoline (DPD), a marker for bone resorption, was significantly elevated in $0.1K^+$ fed mice (Figure 4B). However, no significant differences in osteoid volume, osteoid thickness, osteoblast surface, mineral apposition rate (MAR) or bone formation rate (BFR) were detectable between the diets (Figure 4, C and D). These findings suggest that during dietary K^+ depletion, bone formation and bone mineralization remained unchanged despite increased bone resorption.

Low dietary K^+ intake alters various Ca^{2+} and Pi transport pathways in the kidney. In an attempt to uncover the molecular basis for the increased urinary Ca^{2+} excretion, hypocalcemia and bone resorption during dietary K^+ deficiency, kidney mRNA and protein levels of major regulators of Ca^{2+} and Pi transport (1, 6) were profiled. Initially we focused on the PT, where the majority of kidney Ca^{2+} and virtually all Pi reabsorption occurs. After 4 weeks on the $0.1K^+$ diet, kidney mRNA expression of the genes encoding the Pi transporter Napi2c (*Slc34A2)* and two regulatory proteins, sodium-hydrogen exchanger regulatory factor-1 NHERF-1 (*Slc9a3r1*) and NHERF-3 (*Pdzk1*) (46, 47) were significantly lower compared to $1K^+$ fed mice (Table 1), with NHERF-3 protein levels also reduced (Figure 5). These reductions in mRNA levels persisted at 8 weeks, but similar changes at the protein level were not observed (Figure 5). Napi-2a

(*Slc34a1*) mRNA levels were also reduced after 8-weeks of dietary K^+ restriction (Table 1), but again these did not translate to significant changes in Napi-2a protein levels. NHE3 (*Slc9a3*) mRNA was significantly reduced during prolonged dietary K^+ restriction, but with no major changes observed at the protein level. Furthermore, no changes were observed in the mRNA expression of *Cldn2* and *Cldn12*, the major claudins in the PT mediating paracellular cation transport (Supplemental Table S3) (48). Around 25% of filtered Ca^{2+} is reabsorbed paracellularly in the TAL pathway driven by active Na^+ reabsorption via NKCC2 (15-17, 49). During dietary K^+ restriction, the abundance of phosphorylated T96-NKCC2 (linked to higher activity) was significantly higher, whereas total NKCC2 was lower after 4 weeks (Figure 5). No changes were observed in NKCC2 mRNA (Table 1). The mRNA expression of *Cldn19* was increased after 4 weeks, but no other changes in TAL claudins were observed (Supplemental Table S3). In the DCT, 10% of the filtered Ca^{2+} is reabsorbed by a transcellular pathway (18). Luminal Ca^{2+} enters DCT cells through TRPV5, where it is buffered by calbindin-D28k (CB-D28k) (50), before efflux across the basolateral membrane via the plasma membrane Ca^{2+} ATPase 4 (PMCA4) and/or the Na^+/Ca^{2+} exchanger (NCX1) (51, 52). After feeding mice a $0.1K^+$ diet, mRNA expression of *Slc8a1* (encoding for NCX1) was significantly lower compared to $1K^+$ fed mice (Table 1). *Calb1* (encoding for CB-D28K) and *ATP2B4* (encoding for PMCA4) mRNAs were significantly lower after 8 weeks of dietary K^+ restriction (Table 1), but no differences were detectable at the protein level at this timepoint (Figure 5). After 8 weeks, TRPV5 protein levels were significantly higher in $0.1K^+$ fed mice compared to the $1K^+$ control group (Figure 5). A substantial role, albeit indirectly, for the NaCl co-transporter NCC in the DCT for kidney Ca^{2+} handling is evident from the hypercalciuria observed in patients with genetic defects and hyperactivation of NCC (34), or the greater Ca^{2+} reabsorption observed following NCC inhibition with thiazide diuretics (53, 54). As predicted from previous studies (32), phosphorylated (active) NCC and total NCC protein levels were significantly higher in $0.1K^+$ fed mice compared to the $1K^+$ control group (Figure 5). In addition, dietary K^+ restriction significantly decreased the abundances of the Na^+-independent $Cl^-/HCO3^-$ exchanger pendrin and the vacuolar H^+-ATPase after 4 and 8 weeks, and both the full and cleaved (active) form of αENaC after 8 weeks (Supplemental Figure 5).

Low dietary K^+ intake alters abundance of the calcium-sensing receptor (CaSR). The CaSR is expressed in the TAL, where upon activation it inhibits NKCC2 to promote Ca^{2+} excretion (5, 55). The CaSR is also expressed to a lower extent in the DCT where it activates NCC to enhance NaCl reabsorption (potentially compensating for NKCC2 inhibition), but indirectly it may influence Ca^{2+} handling by this segment (6, 56, 57). After dietary K^+ restriction, CaSR mRNA expression at the whole kidney level was increased (Table 1). To confirm this at the protein level, and address which tubule segment/s any changes occurred in, we performed immunofluorescence double-labeling of the CaSR and NCC on kidney sections from the 4-week study and semi-quantified fluorescence intensity using a deep learning instance segmentation model. In kidneys from the $0.1K^+$ mice, staining intensity of the CaSR in both NCC-positive and NCC-negative tubules was higher relative to $1K^+$ control mice (Figure 6), suggesting greater CaSR in the TAL and DCT during K^+ restriction.

Low dietary K^+ does not increase urinary Ca^{2+} excretion or PTH levels in CA-SPAK mice. Of the significantly changed regulators of Ca^{2+} transport uncovered in study 1 and 2, those expressed in the distal tubule were most consistent, including NCX1, calbindin-D28, uromodulin and the CaSR. Furthermore, phosphorylated (active) NCC and total NCC protein levels were significantly higher in low K^+ fed mice, which is likely to influence Ca^{2+} homeostasis (34, 53, 54). Thus, to assess the potential role of NCC in the low K^+ induced hypercalciuria, in study 3 we fed mice with constitutively high NCC activity, so-called CA-SPAK mice (58, 59), and control mice with a 0.1% K^+ ($0.1K^+$) or 1% K^+ ($1K^+$) diet for 4 weeks and analyzed Ca^{2+} handling parameters (Figure 7A). As seen previously (58), plasma K^+ levels were significantly higher in CA-SPAK mice relative to controls, and although plasma K^+ levels were reduced in both genotypes receiving the $0.1K^+$ diet, plasma K^+ remained higher in the CA-SPAK mice (Figure 7B). In line with this, in CA-SPAK mice on a $1K^+$ intake, urinary FEx K^+ and urinary K^+ excretion were significantly lower relative to controls, although both genotypes reduced their FEx K^+ and urinary K^+ excretion to similar levels during $0.1K^+$ feeding (Figure 7C and Supplemental Figure 6). CA-SPAK mice had significantly lower plasma Ca^{2+} levels than control mice during $1K^+$ feeding, and unlike control mice, this was not significantly

reduced during dietary K^+ restriction (Figure 7B). Concordantly, FEx Ca^{2+} and daily urinary Ca^{2+} excretion were higher in CA-SPAK mice than controls during the $1K^+$ intake, and the low dietary K^+ induced increases observed in control mice were absent (Figure 7C and Supplemental Figure 6). In control mice, plasma PTH levels and urinary DPD excretion were higher after the $0.1K^+$ diet. However, in CA-SPAK on a $1K^+$ diet, PTH levels and urinary DPD excretion were already as high as control mice on the $0.1K^+$ diet, and no significant changes occurred during dietary K^+ restriction (Figure 7, B and C). Together, these data suggest that on a normal $1K^+$ intake, constitutive activation of NCC in CA-SPAK mimics the kidney Ca^{2+} handling phenotype of control mice on a $0.1K^+$ diet, highlighting a role for NCC in maintaining Ca^{2+} homeostasis during dietary K^+ restriction.

Low dietary K^+ intake effects on various Ca^{2+} and Pi transport pathways in CA-SPAK mice. Immunoblotting was used to investigate if there are differences in kidney Ca^{2+} transport pathways in the kidneys of CA-SPAK relative to controls that could explain the differences in their Ca^{2+} handling. As expected, on the $1K^+$ control diet phosphorylated (active) NCC levels (pNCC) were significantly higher in CA-SPAK mice relative to controls (Figure 8). However, dietary K^+ restriction increased pNCC levels in both genotypes to a similar extent. As observed in study 2, the abundances of NHERF3, PMCA4 and calbindin-d28 were reduced with low K^+ intake after 4 weeks in control mice, but these changes were not apparent in the CA-SPAK mice, with their levels already being lower than control mice under normal $1K^+$ intake (Figure 8). Interestingly, a low K^+ intake increased TRPV5 abundance in CA-SPAK mice, whereas this effect was not apparent in the control mice. In addition, dietary K^+ restriction significantly decreased the abundance of αENaC in control mice but not CA-SPAK mice, but no significant differences in pendrin, the H^+-ATPase or Na-K-ATPase were observed between genotypes or conditions (Supplemental Figure 7*)*.

Discussion

Potassium (K^+) is an essential mineral that plays a critical role in fluid and electrolyte balance, nerve transmission, muscle contractions, and cardiovascular health. K^+ balance is also implicated in regulation of Ca^{2+} and Pi homeostasis. Here, our major finding is that dietary K^+ deficiency causes hypercalciuria, hypocalcemia and secondary hyperparathyroidism, leading to reduced trabecular BMD.

Previous studies demonstrated that increasing K^+ intake can positively affect bone metabolism, with a significant positive relationship existing between K^+ intake and BMD (25, 27). For example, K^+-citrate supplementation improved BMD and reduced bone resorption in postmenopausal women (24, 26). This, and other studies have demonstrated *reduced* urinary Ca^{2+} loss subsequent to greater K^+ intake, which is attributed mainly to alterations in systemic acid-base balance (29, 30), predominantly a decrease in the body's acid load and mitigation of metabolic acidosis (24, 26). As hypokalemia can also cause metabolic acidosis, stimulation of PTH secretion and enhanced bone resorption (60-62), it is plausible that the effects of dietary K^+ deficiency observed here are driven by alterations in acid-base balance. However, the normal plasma Cl^- levels in our mice argues against the presence of metabolic acidosis, although we acknowledge that our study is limited by the lack of direct assessment of plasma pH or HCO_3^- levels. Moreover, despite elevated PTH, after 4 and 8 weeks of low dietary K^+ feeding we observed no suppression of renal NaPi2a protein and no increase in urinary fractional phosphate excretion, suggesting a blunted renal response to PTH. These alterations in mineral handling were accompanied by enhanced osteoclast activity and elevations in bone resorption markers, indicating a net shift toward bone loss. Together, these support the notion that dietary K^+ impacts skeletal health through mechanisms beyond just acid-base balance, primarily by modulating renal Ca^{2+} and Pi transport and altering the endocrine signals that govern bone remodeling.

In our initial mass spectrometry discovery studies, feeding mice a diet without K^+ (0 K^+) for 2 weeks resulted in a 3-fold increase in urinary Ca^{2+} excretion, lower plasma Ca^{2+} and an approximate 2-fold increase in plasma PTH levels. This was accompanied by significant reductions in the kidney of the FGF23

coreceptor klotho, NHE3, NKCC2, NCX1, PMCA4 and Napi2a, the functional consequence of which can partly explain the observed hypercalciuria, although the current approach prevents nephron-segment selective changes being determined. In line with the reductions shown here with low dietary K^+, we previously showed an opposing *increase* in klotho, PMCA1 and NCX1 expression in kidneys following high dietary K^+ intake (41). The effects of high dietary K^+ on klotho have also been seen by others (63). Despite similar changes in plasma biochemistries and urine Ca^{2+} excretion after 4 and 8 weeks of dietary K^+ restriction (0.2%K^+), consistent changes in the same transport mechanisms were absent. This suggests either that changes in protein post-translational modification (and activity), protein localization or protein degradation influence renal Ca^{2+} transport in this period, that the renal response to PTH becomes "blunted" over time and a new set-point for PTH effects is reached, or that other mechanisms are involved.

One such mechanism is that the hypokalemic driven increases in NCC activity observed after dietary K^+ restriction could promote urine Ca^{2+} excretion, an idea supported by studies demonstrating that alterations in WNK-SPAK signaling – the major NCC regulatory pathway - modulates Ca^{2+} reabsorption (64). Furthermore, NCC has an inverse correlation to urinary Ca^{2+} excretion and Ca^{2+} balance defects are observed in patients with altered NCC activity (34-36). However, how changes in NCC can translate to changes in renal Ca^{2+} excretion are highly debated. One study suggested that changes in NCC-mediated Na^+ entry into DCT cells alters intracellular Cl^- levels and influences TRPV5-mediated Ca^{2+} flux (54). A second study proposed that activity of the basolateral Na^+/Ca^{2+} exchanger (NCX1) responds to changes in intracellular Na^+ levels, facilitating Ca^{2+} extrusion or reabsorption (65). However, both of these studies focus on *enhanced* Ca^{2+} reabsorption when NCC activity is low, and whether the inverse scenarios exist when NCC activity is high is unknown. A third potential mechanism is that the greater NCC activity during low K^+ intake leads to volume expansion, decreased proximal tubule sodium reabsorption and concurrently reduced paracellular Ca^{2+} reabsorption (65, 66). Such responses in Ca^{2+} excretion have been seen previously when distal tubule sodium reabsorption was enhanced using mineralocorticoids or NaCl loading (67, 68). Interestingly, the abundance of the CaSR in the DCT and the TAL was higher after K^+ restriction, but

whether activation of the CaSR contributes to the changes in NCC (6, 56, 57) and NKCC2 (5, 55) during low dietary K^+ intake is unclear. Furthermore, how NKCC2 phosphorylation (activation) increases under low dietary K^+ intake, whether it is linked to activation of the WNK-SPAK/OSR pathway (69, 70) and why NKCC2 phosphorylation increases despite a reduction in total NKCC2 and the well-established effects of loop diuretics to promote urinary Ca^{2+} excretion (65) requires additional studies.

The hypercalciuria, hypocalcemia, secondary hyperparathyroidism, and trabecular bone loss during low K^+ intake are reciprocal to the phenotype observed when NCC is inhibited. In humans with Gitelman syndrome, areal BMD is often increased due to denser trabecular networks (increased number and decreased thickness), reduced cortical porosity, and higher volumetric BMD, creating a bone microarchitecture that is protective against osteoporosis (71). Mouse models of NCC inactivation show enhanced duodenal Ca^{2+} absorption and increased osteoblast differentiation, alongside hypocalciuria and higher BMD, pointing to both renal and extrarenal drivers of the skeletal phenotype (72, 73). Here, a significant role for NCC in mediating the hypercalciuria and hypocalcemia is supported by the phenotype of CA-SPAK mice, where hyper-activation of NCC during baseline conditions mirrored the phenotype of wildtype mice during dietary K^+ restriction. However, although low dietary K^+ intake increased active phosphorylated NCC levels in both control and CA-SPAK mice by a similar magnitude, a further increase in plasma PTH, urinary Ca^{2+} excretion, and DPD excretion were not observed in CA-SPAK mice. These results were surprising, but we suggest that they are linked to structural distal nephron remodeling in the CA-SPAK mice, with DCT1 expansion and DCT2 and connecting tubule (CNT) atrophy (58). As recent scRNAseq studies suggest that Ca^{2+} reabsorption is particularly prominent in the DCT2 due to higher expression of TRPV5 and CB-D28K (74), the reduced DCT2/CNT volume in CA-SPAK mice may limit their capacity to further respond to changes in NCC activity with changes in Ca^{2+} handling. However, we also cannot rule-out that in CA-SPAK mice there are direct SPAK-mediated effects on Ca^{2+} transport pathways. Additionally, other structural changes secondary to the hypokalemia may occur in the proximal tubule of CA-SPAK mice (75), and changes in proximal tubule metabolism and alpha-ketoglutarate (α-KG)

production (58, 59) could impact Ca^{2+} handling along the kidney tubule. Thus, additional studies in CA-SPAK assessing whether thiazide diuretics reverse the Ca^{2+} handling phenotype would be informative. Furthermore, a key limitation of our study is the absence of BMD measurements in CA-SPAK mice, which would have provided valuable insights into the downstream effects of chronic NCC activation on bone integrity. Future studies incorporating comprehensive skeletal assessments of CA-SPAK or similar models will be important for elucidating whether long-term hyperactivation of NCC will continue to drive urinary Ca^{2+} excretion and alter bone integrity. Furthermore, to strengthen the concept that NCC activation is responsible for the observed phenotype, studies to assess whether bone integrity is altered in NCC knockout mice during low dietary K^+ intake, or during thiazide treatment would be informative.

The hypocalcemia observed after dietary K^+ deficiency was associated with a significant increase in plasma PTH levels, which drives osteoclast activation and bone resorption (4). A notable finding from our histological analyses was significantly increased bone resorption (as evidenced by increased osteoclast numbers and activity) without significant changes in bone formation. This imbalance aligns with clinical observations of secondary hyperparathyroidism, where elevated PTH strongly drives osteoclastogenesis and bone resorption without affecting bone formation (76, 77). Furthermore, sustained PTH elevation due to prolonged dietary K^+ restriction resulted in selective impairment of trabecular bone architecture rather than cortical bone. This is consistent with trabecular bone being more actively remodeled and sensitive to fluctuations in Ca^{2+} homeostasis and hormonal disturbances compared to cortical bone (78, 79). We did not observe a significant reduction in cortical BMD despite an overall reduction in total BMD following low dietary K^+ intake. Instead, we observed a trend toward increased periosteal and endosteal circumference at 4 weeks, which became statistically significant after 8 weeks. These findings suggest that rather than undergoing net mineral loss, the cortical bone compartment may be undergoing compensatory structural remodeling, likely in response to elevated PTH. High levels of PTH stimulate both endosteal resorption and periosteal apposition, processes that can expand cortical cross-sectional area without necessarily reducing overall mineral density (80, 81). This form of bone structural response may maintain cortical BMD despite

systemic mineral imbalance. In contrast, trabecular bone, which lacks the ability to undergo such structural compensation, shows more pronounced loss, contributing to the observed decrease in total BMD. Overall, the preserved cortical BMD in our study likely reflects adaptive periosteal expansion.

FGF23, 1,25(OH)2D, klotho and PTH form a hormonal feedback loop essential for Ca^{2+} and Pi homeostasis (4). PTH stimulates production of active vitamin D by the kidney, which in turn enhances intestinal Ca^{2+} and Pi absorption. 1,25(OH)2D subsequently stimulates bone production of FGF23, which serves as a counter-regulatory hormone that suppresses 1,25(OH)2D and reduces renal Pi reabsorption. FGF23 also inhibits PTH secretion, completing the feedback loop and fine-tuning body mineral balance. However, in this study dietary K^+ restriction had different effects on this axis. In study 1, a $0K^+$ diet for 2 weeks resulted in increased PTH, but also a concordant increase in *cyp27b1* mRNA and 1,25(OH)2D levels. In contrast, prolonged dietary K^+ restriction in study 2 resulted in higher plasma PTH without concurrent changes in FGF23 or 1,25(OH)2D levels. Why these differences occurred remains unclear, but context-dependent interactions have been reported, where changes in one hormone do not always induce changes in another (82-84). For example, in parathyroidectomized mice, PTH administration increased FGF23 levels (85), but the opposite effect was observed in another study (86). Here, the unaltered 1,25(OH)2D levels in study 2 despite secondary hyperparathyroidism are in line with unaltered expression of 1α-hydroxylase (*Cyp27b1*) or 24-hydroxylase (*Cyp24a1*), two major enzymes governing synthesis of 1,25(OH)2D, so altered enzymatic regulation within the vitamin D metabolic pathway seems unlikely. More likely is that after prolonged dietary K^+ restriction, mice develop PTH resistance, which limits 1,25(OH)2D production. Blunted responses to PTH are observed in multiple conditions such as CKD, hyperphosphatemia or magnesium deficiency (87). Supporting partial renal PTH resistance after prolonged dietary K^+ restriction, expression of NHE3 and NaPi2a, both of which are potently inhibited by PTH under normal physiological conditions (6, 9), were reduced after 2 weeks of a K^+ deplete diet, accompanied by greater FEx Pi. However, NHE3, Napi2a and FEx Pi were unchanged after 4 and 8 weeks of a low K^+ diet. The molecular basis of the PTH resistance is unclear, but desensitization of the PTH receptor in bone or kidney due to prolonged

exposure to high PTH levels has been reported (88-91). In line with this, despite high PTH levels in the CA-SPAK mice, they had unchanged urinary and FEx Pi and no significant changes in NaPi-2a or NHE3. However, a limitation of our studies is that we were unable to measure mRNA levels of *Cyp27b1* or *Cyp24a1* or plasma 1,25(OH)2D levels in the CA-SPAK mice from study 3 to strengthen the idea that PTH resistance is also occurring in the model. Further supporting the resistance concept, plasma PTH was chronically elevated in mice with kidney-specific deletion of NHE3, but urinary Pi excretion was unchanged (22). Taken together, our data strongly suggests the presence of renal PTH resistance during prolonged dietary K^+ restriction, but further research is needed to elucidate the molecular mechanisms underlying this blunted PTH response.

Our study is not without additional limitations. Firstly, pNKCC2 levels could not be assessed in CA-SPAK mice as studies in this model were performed prior to the development of a pNKCC2 antibody that was specific in C57Bl/6J mice (92). Secondly, we performed all experiments in male mice and whether similar effects are observed in females needs to be experimentally determined considering there are sex differences in Ca^{2+} and Pi homeostasis (93, 94), renal transporter profiles (95), plasma K^+ concentrations (96) and NCC activity (97). Our studies also do not have direct measurements of intestinal Ca^{2+} and Pi handling, a major limitation considering the role of the intestine in overall Ca^{2+} and Pi homeostasis (48, 98, 99). Although no detectable differences in bodyweight or food intake were observed between the groups in the different studies, this does not equate to unaltered intestinal handling. Future work should specifically examine whether low K^+ intake alters intestinal Ca^{2+} and Pi transport pathways and thereby contributes to Ca^{2+} and Pi homeostasis. Another potential limitation is the level of K^+ used in the dietary regimes. For study 1, the diet was completely deficient in K^+, and although the feeding period was only 2 weeks, such intake is probably never observed in humans. In respect to studies 2 and 3, if correcting between mouse and humans for caloric intake and body weight (100), the 0.1% K^+ intake would be equivalent to ~30 mEq/day (~700 mg). Although this is lower than the average daily K^+ intake of the US population (101), it is within the 10^{th} percentile. For some nationalities, ethnicities or in adolescents the equivalent intake is much closer

to the average daily K^+ consumption (102, 103). Furthermore, in people with eating disorders e.g. anorexia nervosa or inflammatory bowel disease e.g. Crohn's disease or ulcerative colitis, K^+ intake can be very low or gastrointestinal loss very high, which may contribute to osteopenia, osteoporosis and increased fracture risk in these individuals (104, 105).

In summary, our study demonstrates that dietary K^+ deficiency disrupts Ca^{2+} homeostasis, promotes secondary hyperparathyroidism, and leads to reduced trabecular BMD. These insights are important for the prevention and management of mineral and bone disorders in conditions of chronic electrolyte imbalance.

Methods

Sex as a biological variable. All studies were performed in male mice. We expect the findings of our study to also be relevant in females. However, as there are differences in Ca^{2+} homeostasis between sexes and as after menopause females experience a significant drop in estrogen that maintains bone density, similar studies should be repeated in females.

Animal experiments and tissue collection. All diets used in this study were prepared from a base rodent diet (Teklad Diet, TD.88239, Envigo) containing 0.3% Na^+ but being nominally K^+ free. KCl was added back to generate modified diets with different percentages of K^+ (41). Final compositions of the diets used are in Supplemental Table S4. In study 1, 12 weeks old male C57BL/6J mice (Janvier), were housed under standard conditions with a 12/12 hour dark/light cycle (18:00 lights off) and continual free access to water. Mice were randomly assigned a diet containing either 0% ($0.1K^+$) or 1% K^+ control diet ($1K^+$). After 2 weeks, mice were housed individually in metabolic cages (Techniplast) for urine collection, with modified diets and water available *ad libitum*. Subsequently, mice were euthanized by cervical dislocation, kidneys removed and protein homogenates prepared for protein mass spectrometry as previously described (41). In study 2, thirty-two male C57Bl/6J mice of 12-14 weeks of age, were kept in standard cages in a room with a 12:12 hour light/dark cycle with free access to tap water and a standard rodent chow. At the start of the experiment all mice were fed the control 1% K^+ ($1K^+$) diet for 1 week. Subsequently, mice were randomly stratified to either continue on this diet, or receive a diet containing 0.1% K^+ ($0.1K^+$) for 4 or 8 weeks. At the end of the study, mice were housed individually in metabolic cages (Techniplast) for urine collection, with food and water available *ad libitum*. Mice were exsanguinated from the abdominal vena cava under anesthesia with ketamine/xylazine (67 / 7 mg/kg i.p. respectively) for collection of blood plasma. Kidneys were harvested and left femurs were collected and stored in 70% ethanol. In study 3, mice with constitutively active SPS1-related proline/alanine-rich kinase (SPAK) within the distal convoluted tubule (CA-SPAK mice) were used (58). SPAK is a kinase component of the with no lysine kinases (WNK) – SPAK - NCC pathway (32), and the CA-SPAK mice have constitutively high NCC phosphorylation at an

activating site (resulting in high NCC activity) (58, 59). 10-15 weeks old male CA-SPAK or control mice were kept in standard cages in a room with a 12:12 hour light/dark cycle with free access to tap water and a standard rodent chow. Mice were randomly stratified to receive either the control diet containing 1% K^+ or 0.1% K^+. After 4 weeks, mice were housed in metabolic cages for overnight urine collection. Animals were anesthetized by intraperitoneal injection with ketamine/xylazine (100 mg/kg of ketamine, 10 mg/kg of xylazine). Once an animal was unconscious, blood samples were collected from the carotid artery. Kidneys were removed and flash frozen.

Biochemical analyses of plasma and urine. See extended methods in Supplemental Material.

RNA isolation and Quantitative Real-Time PCR (RTqPCR). See extended methods in Supplemental Material. Primer sequences used for RT-qPCR are listed in Supplementary Table S5.

Peripheral quantitative computed tomography (pQCT) and Micro–computed tomography (μCT) analysis. Performed as previously described (106, 107). See extended methods in Supplemental Material.

Bone Histology. Performed as previously described (108-110). See extended methods in Supplemental Material.

Immunoblotting. See extended methods in Supplemental Material. Protein samples and immunoblotting were performed as previously described (111) using well characterized primary antibodies (Supplementary Table S6).

Liquid Chromatography Mass Spectrometry (LC-MS/MS) analysis and bioinformatics. All procedures for sample preparation, instrument parameters, and data processing are described in detail previously (41). See extended methods in Supplemental Material.

Immunofluorescent Labelling and Image Analysis. Mouse kidney tissues from study 2 (4-week timepoint) were labelled as previously described (112, 113) using primary and secondary antibodies (Supplemental Table S6) and DAPI nuclear stain (D1306 Thermo Fisher Scientific). Imaging was

conducted using a Zeiss AxioScan 7 automated slide scanner using a Plan-Apochromat 20x/0.8 M27 (WD=0.55mm) objective under standardized acquisition parameters to ensure consistent exposure across samples. All image acquisition settings were held constant between groups to enable semi-quantitative cross-sample comparisons. Semi-quantitative image analysis was performed with Zeiss Arivis Pro software (version 4.2.1). A deep learning instance segmentation model, custom-trained for this project using the Arivis Cloud platform (*model access token: aoStEkZix4m7hsaOjHkbMYijL29ZvPuLnkZ0G_XkmZA*), was applied to 100% resolution images to achieve accurate renal tubule segmentation. Model performance was validated on held-out images before batch application. Segmentation masks produced by the model enabled extraction of mean fluorescence intensity values for NCC and CaSR signals on a per-tubule basis.

Statistics. Data is plotted as mean ± SEM alongside individual values from independent animals, unless otherwise stated. Individual sample size (n) is shown in figure legends. For comparing two groups of data, data meeting the statistical assumptions of normality were analyzed using a Student's unpaired t-test with level of significance set as 0.05 or below. Comparisons of more than two groups were performed using one- or two-way (regular or repeated measurement) ANOVAs followed by a Dunnett or Tukey multiple comparison test. No samples were excluded from the analysis.

Study Approvals. Study 1 was performed under a license issued by the Danish Animal Experiments Inspectorate; Ministry of Food, Agriculture, and Fisheries; Danish Veterinary and Food Administration (2019-15-0201-00086). Study 2 procedures were approved by the Animal Welfare Committee of the Austrian Federal Ministry of Education, Science and Research (BMWFW-68.205/0188-WF/V/3b/2017). All experiments in study 3 were approved by the Johns Hopkins University Animal Care and Use Committee, USA.

Data availability. Values for all data points in graphs are reported in the Supporting Data Values file. The mass spectrometry data have been deposited to the ProteomeXchange Consortium via the PRIDE partner repository with the data set identifier PXD035354.

Authors contributions. RAF and SKM conceived the study; SKM, MA, XZ, LKR, LNG, RG, AR, RL, JR and QW conducted experiments and acquired data. SKM, RAF, QW, PW, XZ, RGE analyzed and interpreted data. SKM and RAF drafted the manuscript. All authors approved edited and approved the final version of the manuscript.

Acknowledgements. We thank Henrik Dimke (University of Southern Denmark, Odense, Denmark) for the CaSR antibody and Johannes Loffing (Institute of Anatomy, University of Zurich, Switzerland) for the pNKCC2 antibody. We thank Christian Westberg, Inger Merete Paulsen and Cassandra Bennetzen (Aarhus University) for technical support.

Funding. This work was supported by the Novo Nordisk Foundation (NNF21OC0067647, NNF20OC0063837 and NNF24OC0095846 to RAF), the Danish Council for Independent Research (3101-00136B to RAF), and a Leducq Transatlantic Network of Excellence (17CVD05 to RAF and PAW).

Table 1. Relative mRNA expression of genes related to Ca^{2+} and Pi handling in the kidney of mice fed a 1% K^+ ($1K^+$) or 0.1% K^+ ($0.1K^+$) diet for either 4 or 8 weeks (study 2). The relative mRNA abundances are calculated from the Ct values using the delta-delta Ct method. Data are means ± SD. As assessed by unpaired Student's t-test, * = $p < 0.05$, $1K^+$ vs $0.1K^+$ during 4-weeks study (n=8 and 9 respectively) or *b = $p < 0.05$, $1K^+$ vs $0.1K^+$ during 8-weeks study (n = 8 per group).

		4 weeks				**8 weeks**			
		$1K^+$		**$0.1K^+$**		**$1K^+$**		**$0.1K^+$**	
Gene	***Protein name***	***Mean***	***SD***	***Mean***	***SD***	***Mean***	***SD***	***Mean***	***SD***
Atp2b1	PMCA1	1.00	0.22	0.91	0.17	1.00	0.14	1.05	0.13
Atp2b4	PMCA4	1.00	0.27	0.95	0.15	1.00	0.23	0.71*[b]	0.25
Calb1	Calbindin D28	1.00	0.35	0.84	0.35	1.00	0.30	0.66*[b]	0.11
CaSR	CASR	1.00	0.23	1.32*	0.17	1.00	0.09	1.27*[b]	0.32
Pdzk1	NHERF3	1.00	0.14	0.85*	0.09	1.00	0.12	0.85*[b]	0.14
Pvalb	PVALB	1.00	0.12	1.20*	0.09	1.00	0.14	1.28*[b]	0,12
Scnn1a	αENaC	1.00	0.17	0.91	0.21	1.00	0.12	0.86	0.23
Slc8a1	NCX1	1.00	0.09	0.70*	0.13	1.00	0.09	0.75*[b]	0.19
Slc9a3	NHE3	1.00	0.17	0.82*	0.18	1.00	0.18	0.67*[b]	0.25
Slc9a3r1	NHERF1	1.00	0.24	0.79*	0.11	1.00	0.13	0.81*[b]	0.12
Slc12a3	NCC	1.00	0.26	1.05	0.19	1.00	0.22	0.90	0.32
Slc20a2	PiT-2	1.00	0.24	1.03	0.16	1.00	0.16	1.03	0.21
Slc34a1	NaPi-2a	1.00	0.17	0.98	0.14	1.00	0.15	0.78*[b]	0.17
Slc34a3	NaPi-2c	1.00	0.24	0.70*	0.15	1.00	0.20	0.76*[b]	0.16
Slc12a1	NKCC2	1.00	0.68	1.24	0.53	1.00	0.39	0.86	0.48
Trpv5	TRPV5	1.00	0.27	1.13	0.26	1.00	0.21	1.04	0.40

References

1. Blaine J, et al. Renal control of calcium, phosphate, and magnesium homeostasis. *Clin J Am Soc Nephrol.* 2015;10(7):1257-72.
2. Bonjour JP. Calcium and phosphate: a duet of ions playing for bone health. *J Am Coll Nutr.* 2011;30(5 Suppl 1):438S-48S.
3. Bird RP, and Eskin NAM. The emerging role of phosphorus in human health. *Adv Food Nutr Res.* 2021;96:27-88.
4. Blau JE, and Collins MT. The PTH-Vitamin D-FGF23 axis. *Rev Endocr Metab Disord.* 2015;16(2):165-74.
5. Tan RSG, et al. The role of calcium-sensing receptor signaling in regulating transepithelial calcium transport. *Exp Biol Med (Maywood).* 2021;246(22):2407-19.
6. Staruschenko A, et al. Calcium signalling and transport in the kidney. *Nat Rev Nephrol.* 2024;20(8):541-55.
7. Dimke H. New insights into renal calcium-sensing receptor activation. *Curr Opin Nephrol Hypertens.* 2024;33(4):433-40.
8. Beck L, et al. Targeted inactivation of Npt2 in mice leads to severe renal phosphate wasting, hypercalciuria, and skeletal abnormalities. *Proc Natl Acad Sci U S A.* 1998;95(9):5372-7.
9. Blaine J, et al. PTH-induced internalization of apical membrane NaPi2a: role of actin and myosin VI. *Am J Physiol Cell Physiol.* 2009;297(6):C1339-46.
10. Gattineni J, et al. FGF23 decreases renal NaPi-2a and NaPi-2c expression and induces hypophosphatemia in vivo predominantly via FGF receptor 1. *Am J Physiol Renal Physiol.* 2009;297(2):F282-91.
11. Taketani Y, et al. Regulation of type II renal Na+-dependent inorganic phosphate transporters by 1,25-dihydroxyvitamin D3. Identification of a vitamin D-responsive element in the human NAPi-3 gene. *J Biol Chem.* 1998;273(23):14575-81.

12. Friedman PA. Mechanisms of renal calcium transport. *Exp Nephrol.* 2000;8(6):343-50.

13. Schultheis PJ, et al. Renal and intestinal absorptive defects in mice lacking the NHE3 Na+/H+ exchanger. *Nat Genet.* 1998;19(3):282-5.

14. Pan W, et al. The epithelial sodium/proton exchanger, NHE3, is necessary for renal and intestinal calcium (re)absorption. *Am J Physiol Renal Physiol.* 2012;302(8):F943-56.

15. Hebert SC, et al. NaCl transport in mouse medullary thick ascending limbs. I. Functional nephron heterogeneity and ADH-stimulated NaCl cotransport. *Am J Physiol.* 1981;241(4):F412-31.

16. Di Stefano A, et al. Transepithelial Ca2+ and Mg2+ transport in the cortical thick ascending limb of Henle's loop of the mouse is a voltage-dependent process. *Ren Physiol Biochem.* 1993;16(4):157-66.

17. Yu AS. Claudins and the kidney. *J Am Soc Nephrol.* 2015;26(1):11-9.

18. Hoenderop JG, et al. Molecular identification of the apical Ca2+ channel in 1, 25-dihydroxyvitamin D3-responsive epithelia. *J Biol Chem.* 1999;274(13):8375-8.

19. Erben RG. Physiological Actions of Fibroblast Growth Factor-23. *Front Endocrinol (Lausanne).* 2018;9:267.

20. Alexander RT, and Dimke H. Effects of parathyroid hormone on renal tubular calcium and phosphate handling. *Acta Physiol (Oxf).* 2023;238(1):e13959.

21. Bailly C, et al. Stimulation by glucagon and PTH of Ca and Mg reabsorption in the superficial distal tubule of the rat kidney. *Pflugers Arch.* 1985;403(1):28-34.

22. Poulsen SB, et al. Genetic deletion of the kidney sodium/proton exchanger-3 (NHE3) does not alter calcium and phosphate balance due to compensatory responses. *Kidney Int.* 2025;107(2):280-95.

23. Macdonald HM, et al. Effect of potassium citrate supplementation or increased fruit and vegetable intake on bone metabolism in healthy postmenopausal women: a randomized controlled trial. *Am J Clin Nutr.* 2008;88(2):465-74.

24. Granchi D, et al. Potassium citrate prevents increased osteoclastogenesis resulting from acidic conditions: Implication for the treatment of postmenopausal bone loss. *PLoS One.* 2017;12(7):e0181230.

25. Ha J, et al. The association of potassium intake with bone mineral density and the prevalence of osteoporosis among older Korean adults. *Nutr Res Pract.* 2020;14(1):55-61.

26. Jehle S, et al. Partial neutralization of the acidogenic Western diet with potassium citrate increases bone mass in postmenopausal women with osteopenia. *J Am Soc Nephrol.* 2006;17(11):3213-22.

27. Jehle S, et al. Effect of potassium citrate on bone density, microarchitecture, and fracture risk in healthy older adults without osteoporosis: a randomized controlled trial. *J Clin Endocrinol Metab.* 2013;98(1):207-17.

28. Abate V, et al. Potassium Intake and Bone Health: A Narrative Review. *Nutrients.* 2024;16(17).

29. Humalda JK, et al. Effects of Potassium or Sodium Supplementation on Mineral Homeostasis: A Controlled Dietary Intervention Study. *J Clin Endocrinol Metab.* 2020;105(9):e3246-56.

30. Lemann J, Jr., et al. Potassium administration reduces and potassium deprivation increases urinary calcium excretion in healthy adults [corrected]. *Kidney Int.* 1991;39(5):973-83.

31. Hanna RM, et al. Calcium Transport in the Kidney and Disease Processes. *Front Endocrinol (Lausanne).* 2021;12:762130.

32. Hoorn EJ, et al. Regulation of the Renal NaCl Cotransporter and Its Role in Potassium Homeostasis. *Physiol Rev.* 2020;100(1):321-56.

33. Hoover RS, et al. PTH modulation of NCC activity regulates TRPV5 Ca2+ reabsorption. *Am J Physiol Renal Physiol.* 2016;310(2):F144-51.

34. Mayan H, et al. Hypercalciuria in familial hyperkalemia and hypertension accompanies hyperkalemia and precedes hypertension: description of a large family with the Q565E WNK4 mutation. *J Clin Endocrinol Metab.* 2004;89(8):4025-30.

35. Blanchard A, et al. Gitelman syndrome: consensus and guidance from a Kidney Disease: Improving Global Outcomes (KDIGO) Controversies Conference. *Kidney Int.* 2017;91(1):24-33.

36. Mayan H, et al. Hypercalciuria in familial hyperkalemia and hypertension with KLHL3 mutations. *Nephron.* 2015;130(1):59-65.

37. Chuang CH, et al. Association of Thiazide Use in Patients with Hypertension with Overall Fracture Risk: A Population-Based Cohort Study. *J Clin Med.* 2022;11(12).

38. Wang J, et al. Thiazide Diuretics and the Incidence of Osteoporotic Fracture: A Systematic Review and Meta-Analysis of Cohort Studies. *Front Pharmacol.* 2019;10:1364.

39. Sriperumbuduri S, et al. Potassium and Hypertension: A State-of-the-Art Review. *Am J Hypertens.* 2024;37(2):91-100.

40. Fryer JN, et al. Effect of potassium depletion on proximal tubule AT1 receptor localization in normal and remnant rat kidney. *Kidney Int.* 2001;60(5):1792-9.

41. Little R, et al. Dissociation of sodium-chloride cotransporter expression and blood pressure during chronic high dietary potassium supplementation. *JCI Insight.* 2023;8(5).

42. Silver J, and Levi R. Regulation of PTH synthesis and secretion relevant to the management of secondary hyperparathyroidism in chronic kidney disease. *Kidney Int Suppl.* 2005(95):S8-12.

43. Lips P. Vitamin D deficiency and secondary hyperparathyroidism in the elderly: consequences for bone loss and fractures and therapeutic implications. *Endocr Rev.* 2001;22(4):477-501.

44. Abdelhadi M, and Nordenstrom J. Bone mineral recovery after parathyroidectomy in patients with primary and renal hyperparathyroidism. *J Clin Endocrinol Metab.* 1998;83(11):3845-51.

45. Silverberg SJ, et al. Skeletal disease in primary hyperparathyroidism. *J Bone Miner Res.* 1989;4(3):283-91.

46. Villa-Bellosta R, et al. Interactions of the growth-related, type IIc renal sodium/phosphate cotransporter with PDZ proteins. *Kidney Int.* 2008;73(4):456-64.

47. Gisler SM, et al. Interaction of the type IIa Na/Pi cotransporter with PDZ proteins. *J Biol Chem.* 2001;276(12):9206-13.

48. Deluque AL, et al. Biology of calcium homeostasis regulation in intestine and kidney. *Nephrol Dial Transplant.* 2025;40(3):435-45.

49. Ho K, et al. Cloning and expression of an inwardly rectifying ATP-regulated potassium channel. *Nature.* 1993;362(6415):31-8.

50. Kojetin DJ, et al. Structure, binding interface and hydrophobic transitions of Ca2+-loaded calbindin-D(28K). *Nat Struct Mol Biol.* 2006;13(7):641-7.

51. White KE, et al. Structural and functional analysis of Na+/Ca2+ exchange in distal convoluted tubule cells. *Am J Physiol.* 1996;271(3 Pt 2):F560-70.

52. Magyar CE, et al. Plasma membrane Ca2+-ATPase and NCX1 Na+/Ca2+ exchanger expression in distal convoluted tubule cells. *Am J Physiol Renal Physiol.* 2002;283(1):F29-40.

53. Costanzo LS, and Windhager EE. Calcium and sodium transport by the distal convoluted tubule of the rat. *Am J Physiol.* 1978;235(5):F492-506.

54. Gesek FA, and Friedman PA. Mechanism of calcium transport stimulated by chlorothiazide in mouse distal convoluted tubule cells. *J Clin Invest.* 1992;90(2):429-38.

55. Himmerkus N, et al. Calcium-Sensing Receptor in the Thick Ascending Limb and Renal Response to Hypercalcemia. *J Am Soc Nephrol.* 2025;36(6):1028-39.

56. Chavez-Canales M, et al. Regulation of the WNK4-SPAK-NCC pathway by the calcium-sensing receptor. *Curr Opin Nephrol Hypertens.* 2023;32(5):451-7.

57. Bazua-Valenti S, et al. The Calcium-Sensing Receptor Increases Activity of the Renal NCC through the WNK4-SPAK Pathway. *J Am Soc Nephrol.* 2018;29(7):1838-48.

58. Grimm PR, et al. Constitutively Active SPAK Causes Hyperkalemia by Activating NCC and Remodeling Distal Tubules. *J Am Soc Nephrol.* 2017;28(9):2597-606.

59. Grimm PR, et al. Dietary potassium stimulates Ppp1Ca-Ppp1r1a dephosphorylation of kidney NaCl cotransporter and reduces blood pressure. *J Clin Invest.* 2023;133(21).

60. Bichara M, et al. Acute metabolic acidosis enhances circulating parathyroid hormone, which contributes to the renal response against acidosis in the rat. *J Clin Invest.* 1990;86(2):430-43.

61. Lopez I, et al. Direct effect of acute metabolic and respiratory acidosis on parathyroid hormone secretion in the dog. *J Bone Miner Res.* 2002;17(9):1691-700.

62. Krieger NS, et al. Mechanism of acid-induced bone resorption. *Curr Opin Nephrol Hypertens.* 2004;13(4):423-36.

63. Jung HJ, et al. Klotho is highly expressed in the chief sites of regulated potassium secretion, and it is stimulated by potassium intake. *Sci Rep.* 2024;14(1):10740.

64. Hadchouel J, et al. Regulation of Renal Electrolyte Transport by WNK and SPAK-OSR1 Kinases. *Annu Rev Physiol.* 2016;78:367-89.

65. Alexander RT, and Dimke H. Effect of diuretics on renal tubular transport of calcium and magnesium. *Am J Physiol Renal Physiol.* 2017;312(6):F998-F1015.

66. Nijenhuis T, et al. Thiazide-induced hypocalciuria is accompanied by a decreased expression of Ca2+ transport proteins in kidney. *Kidney Int.* 2003;64(2):555-64.

67. Poujeol P, et al. Influence of extracellular fluid volume expansion on magnesium, calcium and phosphate handling along the rat nephron. *Pflugers Arch.* 1976;365(2-3):203-11.

68. Suki WN, et al. Effect of chronic mineralocorticoid administration on calcium excretion in the rat. *Am J Physiol.* 1968;215(1):71-4.

69. Ostroverkhova DS, et al. Calcium-Sensing Receptor and Regulation of WNK Kinases in the Kidney. *Cells.* 2020;9(7).

70. Ponce-Coria J, et al. Regulation of NKCC2 by a chloride-sensing mechanism involving the WNK3 and SPAK kinases. *Proc Natl Acad Sci U S A.* 2008;105(24):8458-63.

71. Qi W, et al. Na-Cl Co-transporter (NCC) gene inactivation is associated with improved bone microstructure. *Osteoporos Int.* 2022;33(10):2193-204.

72. Hsu YJ, et al. Thiazide-sensitive Na+ -Cl- cotransporter (NCC) gene inactivation results in increased duodenal Ca2+ absorption, enhanced osteoblast differentiation and elevated bone mineral density. *J Bone Miner Res.* 2015;30(1):116-27.

73. Nicolet-Barousse L, et al. Inactivation of the Na-Cl co-transporter (NCC) gene is associated with high BMD through both renal and bone mechanisms: analysis of patients with Gitelman syndrome and Ncc null mice. *J Bone Miner Res.* 2005;20(5):799-808.

74. Su XT, et al. Enriched Single-Nucleus RNA-Sequencing Reveals Unique Attributes of Distal Convoluted Tubule Cells. *J Am Soc Nephrol.* 2024;35(4):426-40.

75. Harris AN, et al. Mechanism of Hyperkalemia-Induced Metabolic Acidosis. *J Am Soc Nephrol.* 2018;29(5):1411-25.

76. Rolighed L, et al. Bone Involvement in Primary Hyperparathyroidism and Changes After Parathyroidectomy. *Eur Endocrinol.* 2014;10(1):84-7.

77. Yajima A, et al. Changes of bone remodeling immediately after parathyroidectomy for secondary hyperparathyroidism. *Am J Kidney Dis.* 2003;42(4):729-38.

78. Bennell KL, et al. Skeletal effects of menstrual disturbances in athletes. *Scand J Med Sci Sports.* 1997;7(5):261-73.

79. Bjornerem A, et al. Menopause-Related Appendicular Bone Loss is Mainly Cortical and Results in Increased Cortical Porosity. *J Bone Miner Res.* 2018;33(4):598-605.

80. Rubin MR, and Bilezikian JP. Parathyroid hormone as an anabolic skeletal therapy. *Drugs.* 2005;65(17):2481-98.

81. Rhee Y, et al. Resorption controls bone anabolism driven by parathyroid hormone (PTH) receptor signaling in osteocytes. *J Biol Chem.* 2013;288(41):29809-20.

82. Lavi-Moshayoff V, et al. PTH increases FGF23 gene expression and mediates the high-FGF23 levels of experimental kidney failure: a bone parathyroid feedback loop. *Am J Physiol Renal Physiol.* 2010;299(4):F882-9.

83. Liu S, et al. Fibroblast growth factor 23 is a counter-regulatory phosphaturic hormone for vitamin D. *J Am Soc Nephrol.* 2006;17(5):1305-15.

84. Saji F, et al. Fibroblast growth factor 23 production in bone is directly regulated by 1alpha,25-dihydroxyvitamin D, but not PTH. *Am J Physiol Renal Physiol.* 2010;299(5):F1212-7.

85. Lopez I, et al. Direct and indirect effects of parathyroid hormone on circulating levels of fibroblast growth factor 23 in vivo. *Kidney Int.* 2011;80(5):475-82.

86. Samadfam R, et al. Bone formation regulates circulating concentrations of fibroblast growth factor 23. *Endocrinology.* 2009;150(11):4835-45.

87. Evenepoel P, et al. Parathyroid hormone metabolism and signaling in health and chronic kidney disease. *Kidney Int.* 2016;90(6):1184-90.

88. Pun KK, et al. Desensitization of parathyroid hormone receptors on cultured bone cells. *J Bone Miner Res.* 1990;5(12):1193-200.

89. Fukayama S, et al. Mechanisms of desensitization to parathyroid hormone in human osteoblast-like SaOS-2 cells. *Endocrinology.* 1992;131(4):1757-69.

90. Fujimori A, et al. Desensitization of calcium messenger system in parathyroid hormone-stimulated opossum kidney cells. *Am J Physiol.* 1993;264(6 Pt 1):E918-24.

91. Bergwitz C, et al. Rapid desensitization of parathyroid hormone dependent adenylate cyclase in perifused human osteosarcoma cells (SaOS-2). *Biochim Biophys Acta.* 1994;1222(3):447-56.

92. Moser S, et al. A five amino acids deletion in NKCC2 of C57BL/6 mice affects analysis of NKCC2 phosphorylation but does not impact kidney function. *Acta Physiol (Oxf).* 2021;233(1):e13705.

93. Stadt MM, and Layton AT. Mathematical modeling of calcium homeostasis in female rats: An analysis of sex differences and maternal adaptations. *J Theor Biol.* 2023;572:111583.

94. Bosman A, et al. Sexual dimorphisms in serum calcium and phosphate concentrations in the Rotterdam Study. *Sci Rep.* 2023;13(1):8310.

95. McDonough AA, and Layton AT. Sex differences in renal electrolyte transport. *Curr Opin Nephrol Hypertens.* 2023;32(5):467-75.

96. Wysowski DK, et al. Sex and age differences in serum potassium in the United States. *Clin Chem.* 2003;49(1):190-2.

97. Chen Z, et al. Influence of gender on renal thiazide diuretic receptor density and response. *J Am Soc Nephrol.* 1994;5(4):1112-9.

98. Wagner CA. The basics of phosphate metabolism. *Nephrol Dial Transplant.* 2024;39(2):190-201.

99. Beggs MR, et al. The contribution of regulated colonic calcium absorption to the maintenance of calcium homeostasis. *J Steroid Biochem Mol Biol.* 2022;220:106098.

100. Assmus AM, et al. Excess dietary potassium raises blood pressure in male mice by an aldosterone-dependent increase in ENaC. *Communications Biology.* 2025.

101. Cogswell ME, et al. Sodium and potassium intakes among US adults: NHANES 2003-2008. *Am J Clin Nutr.* 2012;96(3):647-57.

102. Rios-Leyvraz M, et al. Worldwide and time trends in sodium and potassium intakes in children and adolescents: a systematic review and meta-analysis. *BMJ Nutr Prev Health.* 2025;8(1):e001016.

103. Reddin C, et al. Global mean potassium intake: a systematic review and Bayesian meta-analysis. *Eur J Nutr.* 2023;62(5):2027-37.

104. Marzban Abbas Abadi M, et al. Prevalence of osteoporosis in patients with inflammatory bowel disease: a systematic review and meta-analysis. *J Health Popul Nutr.* 2025;44(1):178.

105. Fazeli PK, and Klibanski A. Effects of Anorexia Nervosa on Bone Metabolism. *Endocr Rev.* 2018;39(6):895-910.

106. Poulsen SB, et al. Genetic deletion of the kidney sodium/proton exchanger-3 (NHE3) does not alter calcium and phosphate balance due to compensatory responses. *Kidney Int.* 2024.

107. Schneider MR, et al. Normal epidermal growth factor receptor signaling is dispensable for bone anabolic effects of parathyroid hormone. *Bone.* 2012;50(1):237-44.

108. Erben RG. Embedding of bone samples in methylmethacrylate: an improved method suitable for bone histomorphometry, histochemistry, and immunohistochemistry. *J Histochem Cytochem.* 1997;45(2):307-13.

109. Erben RG, and Glosmann M. Histomorphometry in Rodents. *Methods Mol Biol.* 2019;1914:411-35.

110. Schenk R, et al.: Elsevier Science Publishers BV Amsterdam–New York–Oxford; 1984.

111. Murali SK, et al. The Deubiquitylase USP4 Interacts with the Water Channel AQP2 to Modulate Its Apical Membrane Accumulation and Cellular Abundance. *Cells.* 2019;8(3).

112. Poulsen SB, et al. Role of adenylyl cyclase 6 in the development of lithium-induced nephrogenic diabetes insipidus. *JCI Insight.* 2017;2(7):e91042.

113. Poulsen SB, et al. Adenylyl cyclase 6 is required for maintaining acid-base homeostasis. *Clin Sci (Lond).* 2018;132(16):1779-96.

Figure 1. A K^+ deficient diet for two weeks alters kidney Ca^{2+} and Pi handling proteins. (A) Study 1; Experimental overview where mice were fed a control diet containing 1% K^+ ($1K^+$) or a diet deficient in K^+ ($0K^+$) for 2 weeks. Created in Biorender. **(B)** Plasma concentrations of sodium (Na^+), potassium (K^+), chloride (Cl^-) total calcium (Ca^{2+}), phosphate (Pi), PTH and VitD (1,25(OH)2D or calcitriol). **(C)** Urinary fractional excretion of same ions, creatine clearance and daily aldosterone excretion. Each data point arises from an individual mouse and the bars represent group mean ± SEM. Statistical analyses were performed using a Student's unpaired t-test and annotations represent the level of significance. **(D)** Kidney samples were examined using quantitative proteomics. The volcano plot shows the distribution of all quantifiable proteins. X-axis is the Log2 ratio between $1K^+$ and $0K^+$ diets, while Y-axis represents the significance level of the ratio. Significantly changed proteins were defined using a Benjamini-Hochberg false discovery rate of 5%. Proteins (genes names shown) highlighted in blue are examples of proteins involved in Ca^{2+} handling, proteins in green are involved in Pi handling, and red means involvement in both. **(E)** Ingenuity pathway analysis on significantly changed proteins. Lower X-axis is the ratio of proteins (genes) that are involved in this pathway versus the total input, while upper X-axis is the significance level determined by Fisher's exact test. Color of bars represent either promotion (positive z-score) or inhibition (negative z-score) of the pathway. Canonical pathways under the category "Intracellular and Second Messenger Signaling" were plotted with a cutoff of 0.5 on both minus log(p value by Fisher's exact test) and absolute value of z-score.

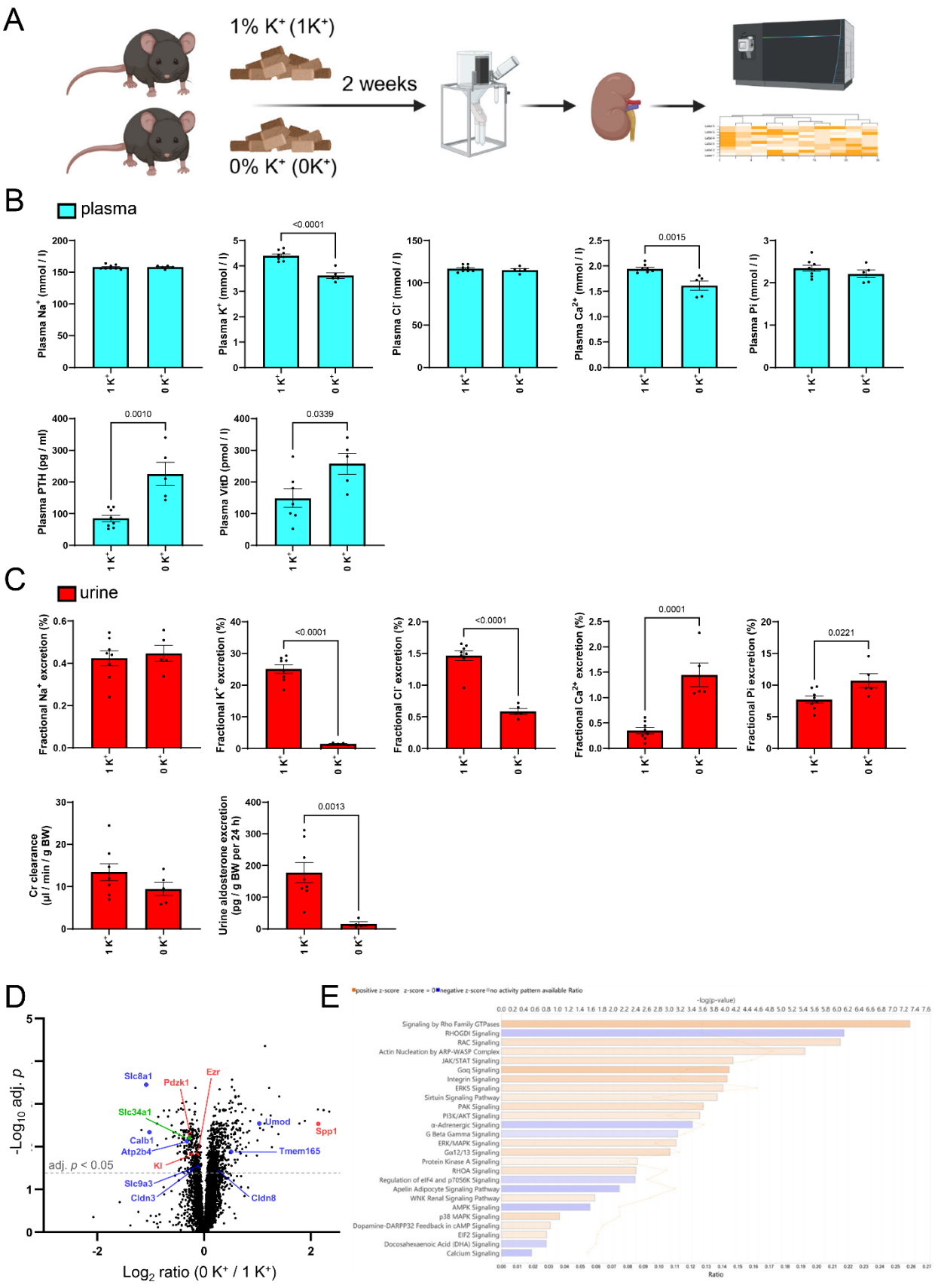
A
1% K⁺ (1K⁺)
2 weeks
0% K⁺ (0K⁺)
B
plasma
Plasma Na⁺ (mmol / l)
Plasma K⁺ (mmol / l)
<0.0001
Plasma Cl⁻ (mmol / l)
Plasma Ca²⁺ (mmol / l)
0.0015
Plasma Pi (mmol / l)
Plasma PTH (pg / ml)
0.0010
Plasma VitD (pmol / l)
0.0339
1 K⁺
0 K⁺
C
urine
Fractional Na⁺ excretion (%)
Fractional K⁺ excretion (%)
<0.0001
Fractional Cl⁻ excretion (%)
<0.0001
Fractional Ca²⁺ excretion (%)
0.0001
Fractional Pi excretion (%)
0.0221
Cr clearance (µl / min / g BW)
Urine aldosterone excretion (pg / g BW per 24 h)
0.0013
D
-Log10 adj. p
adj. p < 0.05
Slc8a1
Pdzk1
Ezr
Slc34a1
Umod
Spp1
Calb1
Atp2b4
Tmem165
Kl
Slc9a3
Cldn3
Cldn8
Log2 ratio (0 K⁺ / 1 K⁺)
E
positive z-score
z-score = 0
negative z-score
no activity pattern available
Ratio
Signaling by Rho Family GTPases
RHOGDI Signaling
RAC Signaling
Actin Nucleation by ARP-WASP Complex
JAK/STAT Signaling
Gαq Signaling
Integrin Signaling
ERK5 Signaling
Sirtuin Signaling Pathway
PAK Signaling
PI3K/AKT Signaling
α-Adrenergic Signaling
G Beta Gamma Signaling
ERK/MAPK Signaling
Gα12/13 Signaling
Protein Kinase A Signaling
RHOA Signaling
Regulation of eIF4 and p70S6K Signaling
Apelin Adipocyte Signaling Pathway
WNK Renal Signaling Pathway
AMPK Signaling
p38 MAPK Signaling
Dopamine-DARPP32 Feedback in cAMP Signaling
EIF2 Signaling
Docosahexaenoic Acid (DHA) Signaling
Calcium Signaling

Figure 2. Prolonged low dietary K^+ intake results in higher urinary Ca^{2+} excretion, hypocalcemia and greater plasma PTH levels. (A) Study 2; Experimental overview of mice maintained on either a low 0.1% K^+ diet ($0.1K^+$) or a normal 1% K^+ diet ($1K^+$) across two independent studies, each lasting either 4 weeks (blue bars) or 8 weeks (red bars). Created in Biorender. **(B)** Analysis of plasma electrolytes. Calcium (Ca^{2+}) is total plasma Ca^{2+}. **(C)** Urinary fractional excretion of ions, creatine (cr) clearance and daily aldosterone excretion. **(D)** Analysis of plasma hormones. VitD = 1,25(OH)2D (calcitriol). For all panels, each data point arises from an individual mouse and the bars represent group mean ± SEM (n=8 in each group). Statistical analyses were performed using a Student's unpaired t-test and annotations between bars represent the level of significance.

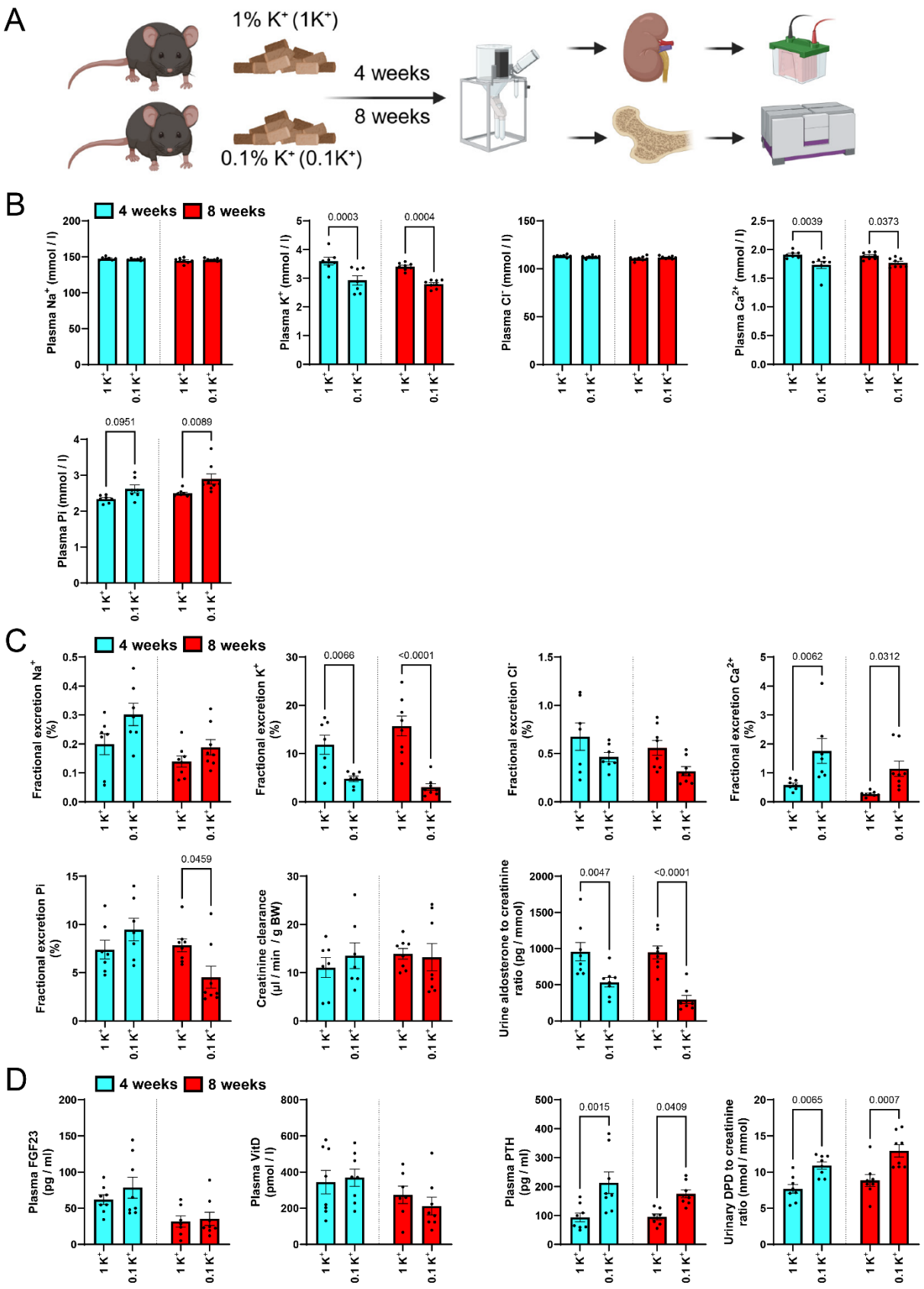
A
1% K+ (1K+)
4 weeks
8 weeks
0.1% K+ (0.1K+)
B
4 weeks
8 weeks
Plasma Na+ (mmol / l)
Plasma K+ (mmol / l)
0.0003
0.0004
Plasma Cl- (mmol / l)
Plasma Ca2+ (mmol / l)
0.0039
0.0373
Plasma Pi (mmol / l)
0.0951
0.0089
1 K+
0.1 K+
C
4 weeks
8 weeks
Fractional excretion Na+ (%)
Fractional excretion K+ (%)
0.0066
<0.0001
Fractional excretion Cl- (%)
Fractional excretion Ca2+ (%)
0.0062
0.0312
Fractional excretion Pi (%)
0.0459
Creatinine clearance (µl / min / g BW)
Urine aldosterone to creatinine ratio (pg / mmol)
0.0047
<0.0001
D
4 weeks
8 weeks
Plasma FGF23 (pg / ml)
Plasma VitD (pmol / l)
Plasma PTH (pg / ml)
0.0015
0.0409
Urinary DPD to creatinine ratio (nmol / mmol)
0.0065
0.0007
1 K+
0.1 K+

Figure 3. Dietary K^+ restriction results in progressive loss of trabecular bone and reduced total BMD in the femoral midshaft and metaphysis. Bone was assessed from mice that were maintained on either a low 0.1% K^+ diet ($0.1K^+$) or a normal 1% K^+ diet ($1K^+$) across two independent studies, each lasting either 4 weeks (blue bars) or 8 weeks (red bars). **(A)** Peripheral quantitative computed tomography (pQCT) was used to measure in the proximal femoral metaphysis the periosteal and endosteal circumference, the total BMD and the trabecular BMD. **(B)** Representative bone femoral shaft cross sectional images using pQCT. **(C)** Total BMD, cortical BMD, cortical thickness, periosteal and endosteal circumference of the femoral shaft assessed using pQCT. **(D)** Trabecular number, thickness, spacing and BMD of the proximal femoral metaphysis was measured using quantitative microcomputed tomography (μ-QCT). **(E)** Total BMD, cortical BMD and cortical thickness of the femoral shaft measured using μ-QCT. For all panels, each data point arises from an individual mouse and the bars represent group mean ± SEM (n=8 in each group). Statistical analyses were performed using a Student's unpaired t-test.

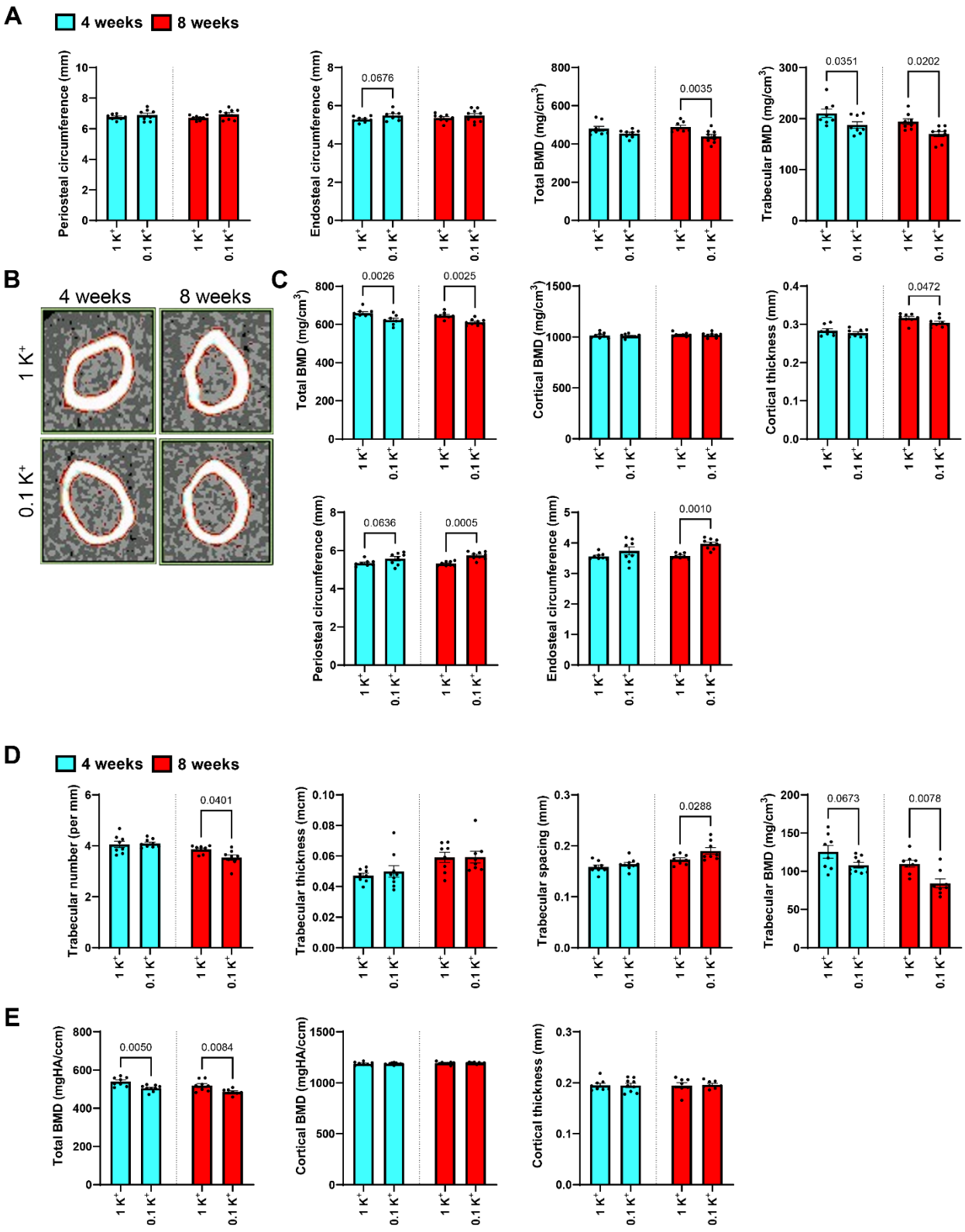
A
4 weeks
8 weeks
Periosteal circumference (mm)
Endosteal circumference (mm)
Total BMD (mg/cm3)
Trabecular BMD (mg/cm3)
0.0676
0.0035
0.0351
0.0202
B
4 weeks
8 weeks
1 K+
0.1 K+
C
Total BMD (mg/cm3)
Cortical BMD (mg/cm3)
Cortical thickness (mm)
Periosteal circumference (mm)
Endosteal circumference (mm)
0.0026
0.0025
0.0472
0.0636
0.0005
0.0010
D
Trabecular number (per mm)
Trabecular thickness (mcm)
Trabecular spacing (mm)
Trabecular BMD (mg/cm3)
0.0401
0.0288
0.0673
0.0078
E
Total BMD (mgHA/ccm)
Cortical BMD (mgHA/ccm)
Cortical thickness (mm)
0.0050
0.0084

Figure 4. Increased osteoclast number and surface during lower dietary K^+ intake. Non-decalcified sections of proximal femur were assessed from mice that were maintained on either a low 0.1% K^+ diet ($0.1K^+$) or a normal 1% K^+ diet ($1K^+$) for 4 weeks (blue bars) or 8 weeks (red bars). **(A)** Representative images of TRACP staining and corresponding quantification of osteoclast surface normalized to bone surface (Oc.S/BS %) and osteoclast number per mm of bone surface (N. Oc/B.pm / mm). **(B)** Urinary excretion of deoxypyridinoline (DPD), a marker for bone resorption. **(C)** Representative images of similar sections stained for von Kossa/McNeal and corresponding quantification of osteoid volume per bone volume (OV/BV), osteoid thickness, osteoblast surface per bone surface (Ob.S/BS) and bone surface per total bone volume (BS/TV). **(D)** Quantification from double calcein labeling analysis of undecalcified sections of proximal femur. Mineral apposition rate (MAR) per day or bone formation rate per bone surface per day (BFR/BS) is shown. For all panels, each data point arises from an individual mouse and the bars represent group mean ± SEM (n=8 in each group). Statistical analyses were performed using a Student's unpaired t-test and annotations between bars represent the level of significance.

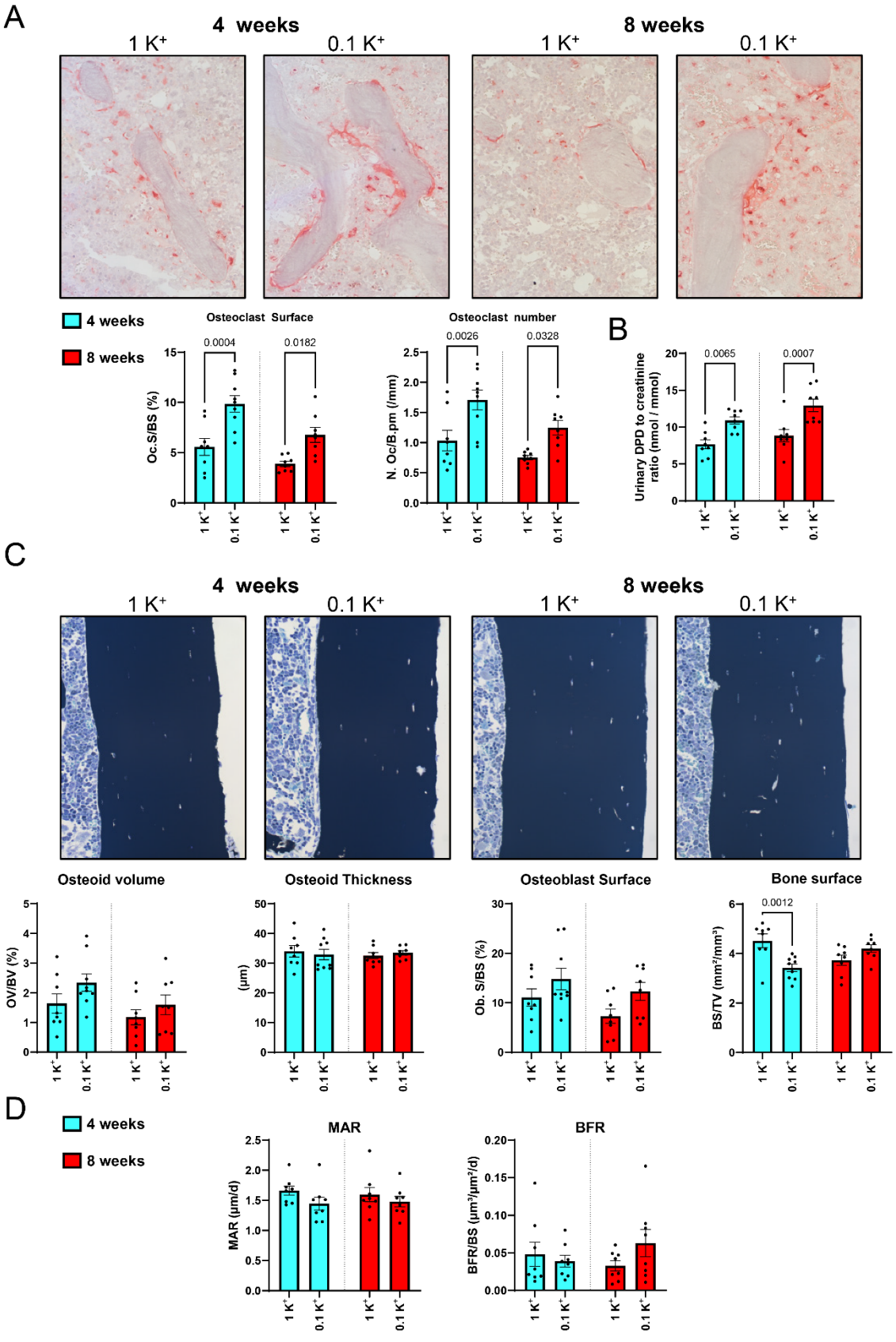
A
4 weeks
8 weeks
1 K+
0.1 K+
4 weeks
8 weeks
Osteoclast Surface
Oc.S/BS (%)
0.0004
0.0182
Osteoclast number
N. Oc/B.pm (/mm)
0.0026
0.0328
B
Urinary DPD to creatinine ratio (nmol / mmol)
0.0065
0.0007
C
Osteoid volume
OV/BV (%)
Osteoid Thickness
(µm)
Osteoblast Surface
Ob. S/BS (%)
Bone surface
BS/TV (mm²/mm³)
0.0012
D
MAR
MAR (µm/d)
BFR
BFR/BS (µm³/µm²/d)

Figure 5. Low dietary K^+ effects on various modulators of Ca^{2+}, Pi and Na^+ transport in the kidney. Immunoblotting of kidney samples from mice that were maintained on either a low 0.1% K^+ diet ($0.1K^+$) or a normal 1% K^+ diet ($1K^+$) across two independent studies, each lasting either 4 weeks (blue bars) or 8 weeks (red bars). **(A)** Representative immunoblots of NaPi2a, NHERF1, NHERF3, TRPV5, Calbindin-28K (CB-D28K), PMCA4, Parvalbumin (PVALB), NHE3, phosphorylated T96 NKCC2 (pNKCC2), NKCC2, phosphorylated T58 NCC (pNCC), NCC and proteasome 20s (P20s, loading control) from 4-weeks study. **(B)** Representative immunoblots from 8-weeks study. **(C)** Summarized relative densitometry data. For all panels, each data point arises from an individual mouse and the bars represent group mean ± SEM (n=8 in each group). Statistical analyses were performed using a Student's unpaired t-test and annotations between bars represent the level of significance.

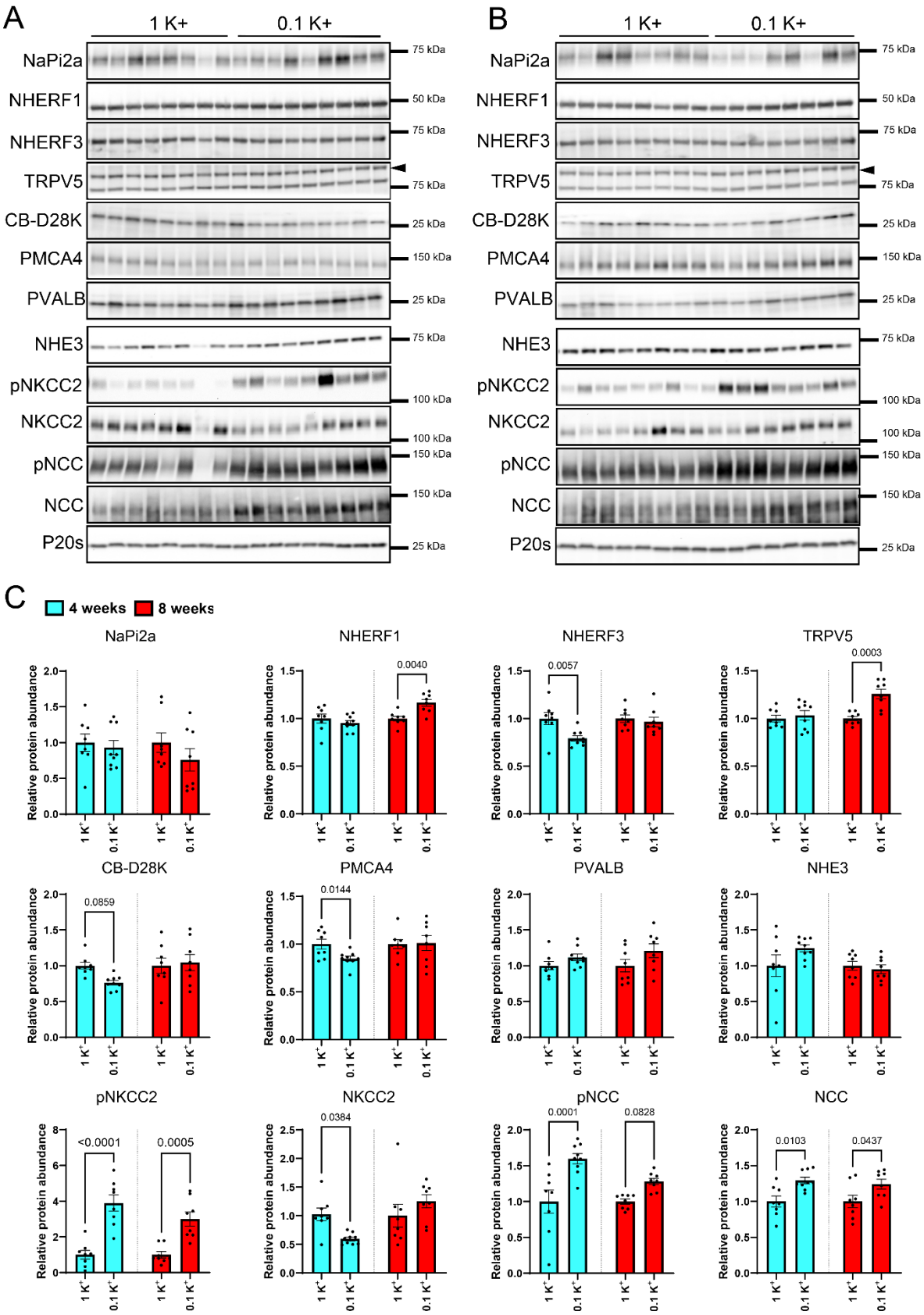
A
1 K+
0.1 K+
NaPi2a
NHERF1
NHERF3
TRPV5
CB-D28K
PMCA4
PVALB
NHE3
pNKCC2
NKCC2
pNCC
NCC
P20s
75 kDa
50 kDa
75 kDa
75 kDa
25 kDa
150 kDa
25 kDa
75 kDa
100 kDa
100 kDa
150 kDa
150 kDa
25 kDa
B
1 K+
0.1 K+
NaPi2a
NHERF1
NHERF3
TRPV5
CB-D28K
PMCA4
PVALB
NHE3
pNKCC2
NKCC2
pNCC
NCC
P20s
75 kDa
50 kDa
75 kDa
75 kDa
25 kDa
150 kDa
25 kDa
75 kDa
100 kDa
100 kDa
150 kDa
150 kDa
25 kDa
C
4 weeks
8 weeks
NaPi2a
NHERF1
NHERF3
TRPV5
CB-D28K
PMCA4
PVALB
NHE3
pNKCC2
NKCC2
pNCC
NCC
Relative protein abundance
0.0040
0.0057
0.0003
0.0859
0.0144
<0.0001
0.0005
0.0384
0.0001
0.0828
0.0103
0.0437
1 K+
0.1 K+

Figure 6. Low dietary K^+ intake alters abundance of the calcium-sensing receptor (CaSR). (A) Representative immunofluorescence images of DAPI nuclear (blue), NCC (green) and CaSR (red) staining in kidney tissue from mice receiving a $1K^+$ or $0.1K^+$ diet for 4 weeks. **(B)** Higher magnification images and example of deep learning instance segmentation model to identify kidney tubules. **(C)** Semi-quantification of CaSR fluorescence intensity in NCC-negative (NCC-) and NCC-positive (NCC+) tubules indicates that CaSR levels are higher in kidneys of mice after $0.1K^+$ relative to $1K^+$ control mice. Each dot represents mean signal intensity in an individual tubule and bars represent median ± interquartile range. n = 4 mice/group. Statistical comparisons were performed using the Mann–Whitney U test. ***$p < 0.001$, ****$p < 0.0001$. Scale bar: 50 μm.

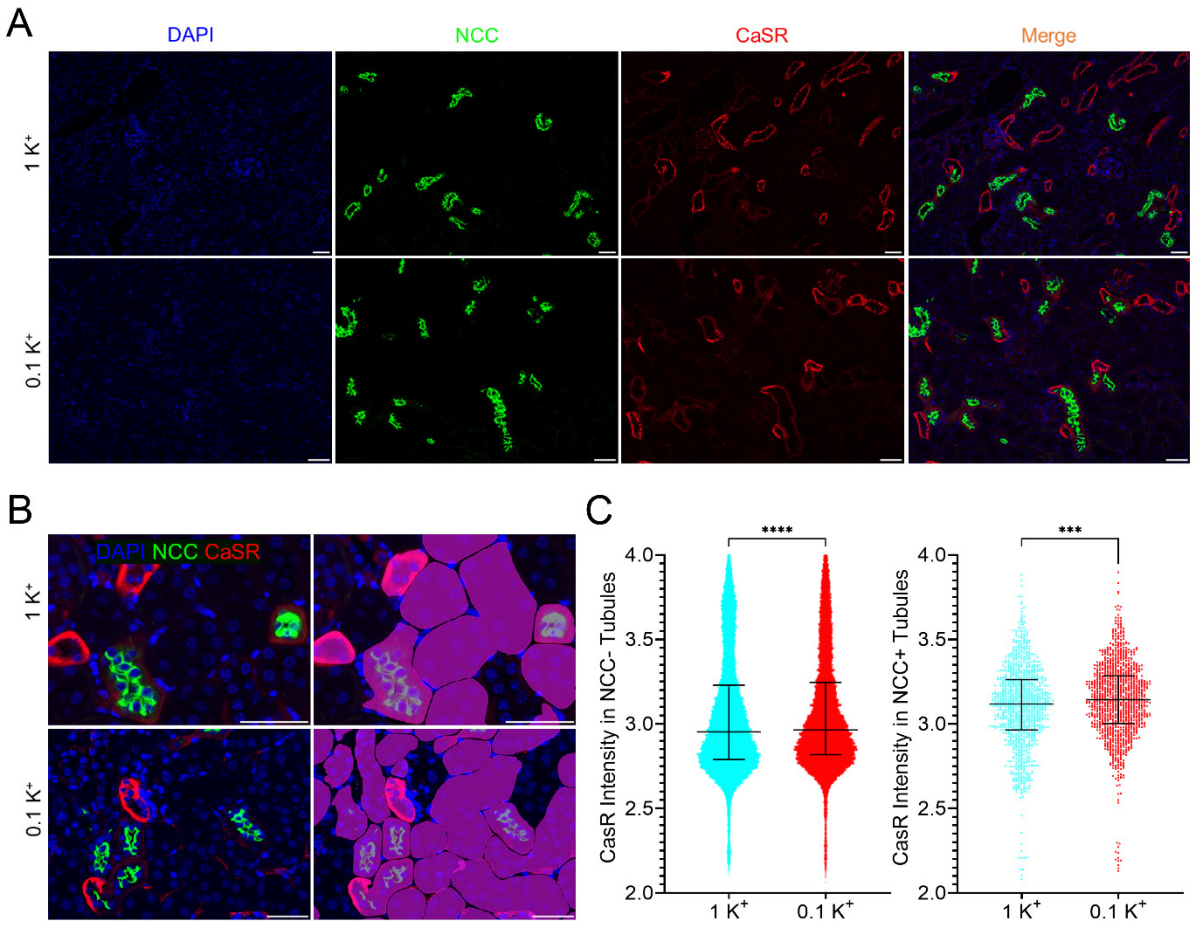
A
DAPI
NCC
CaSR
Merge
1 K+
0.1 K+
B
DAPI NCC CaSR
1 K+
0.1 K+
C
CasR Intensity in NCC- Tubules
CasR Intensity in NCC+ Tubules
4.0
3.5
3.0
2.5
2.0
****
***
1 K+
0.1 K+

Figure 7. Low dietary K^+ does not increase urinary Ca^{2+} excretion or PTH levels in CA-SPAK mice. **(A)**; Overview of experimental approach in study 3 where control (blue bars) or CA-SPAK mice (model with hyperactivation of NCC, red bars) were maintained on either a low 0.1% K^+ diet ($0.1K^+$) or a normal 1% K^+ diet ($1K^+$) for 4 weeks. Created in Biorender. **(B)** Analysis of plasma electrolytes and PTH. **(C)** Urinary fractional excretion of ions, creatine clearance and DPD excretion. For all panels, each data point arises from an individual mouse and the bars represent group mean ± SEM (n=5 for controls and n=7 for CA-SPAK). Statistical analyses were performed using a two-way ANOVA followed by a Tukey multiple comparison test. Annotations between bars represent the level of significance.

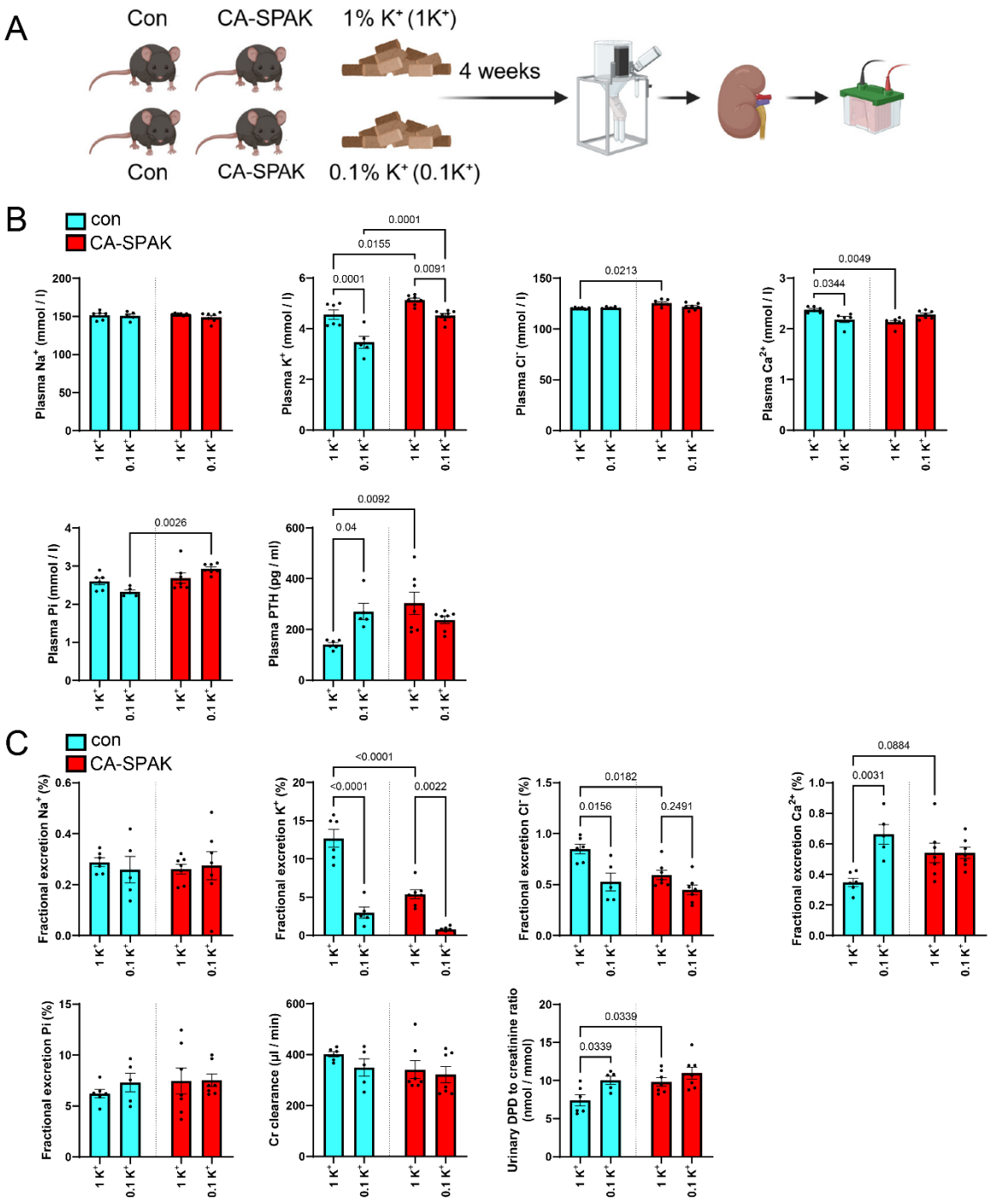
A
Con
CA-SPAK
1% K+ (1K+)
4 weeks
Con
CA-SPAK
0.1% K+ (0.1K+)
B
con
CA-SPAK
Plasma Na+ (mmol / l)
Plasma K+ (mmol / l)
0.0001
0.0155
0.0001
0.0091
Plasma Cl- (mmol / l)
0.0213
Plasma Ca2+ (mmol / l)
0.0049
0.0344
Plasma Pi (mmol / l)
0.0026
Plasma PTH (pg / ml)
0.0092
0.04
1 K+
0.1 K+
C
con
CA-SPAK
Fractional excretion Na+ (%)
Fractional excretion K+ (%)
<0.0001
<0.0001
0.0022
Fractional excretion Cl- (%)
0.0182
0.0156
0.2491
Fractional excretion Ca2+ (%)
0.0884
0.0031
Fractional excretion Pi (%)
Cr clearance (µl / min)
Urinary DPD to creatinine ratio (nmol / mmol)
0.0339
0.0339

Figure 8. Low dietary K^+ effects on various modulators of Ca^{2+}, Pi and Na^+ transport in the kidney of CA-SPAK mice or controls. Immunoblotting of kidney samples from control (blue bars) or CA-SPAK mice (red bars) that were maintained on either a low 0.1% K^+ diet ($0.1K^+$) or a normal 1% K^+ diet ($1K^+$) for 4 weeks. **(A)** Representative immunoblots of NaPi2a, NHERF1, NHERF3, TRPV5, Calbindin-28K (CB-D28K), PMCA4, Parvalbumin (PVALB), NHE3, NKCC2, phosphorylated T58 NCC (pNCC), NCC and proteasome 20s (P20s, loading control). **(B)** Summarized relative densitometry data. For all panels, each data point arises from an individual mouse and the bars represent group mean ± SEM (n=5 for controls and n=7 for CA-SPAK). Statistical analyses were performed using a two-way ANOVA followed by a Tukey multiple comparison test. Annotations between bars represent the level of significance.

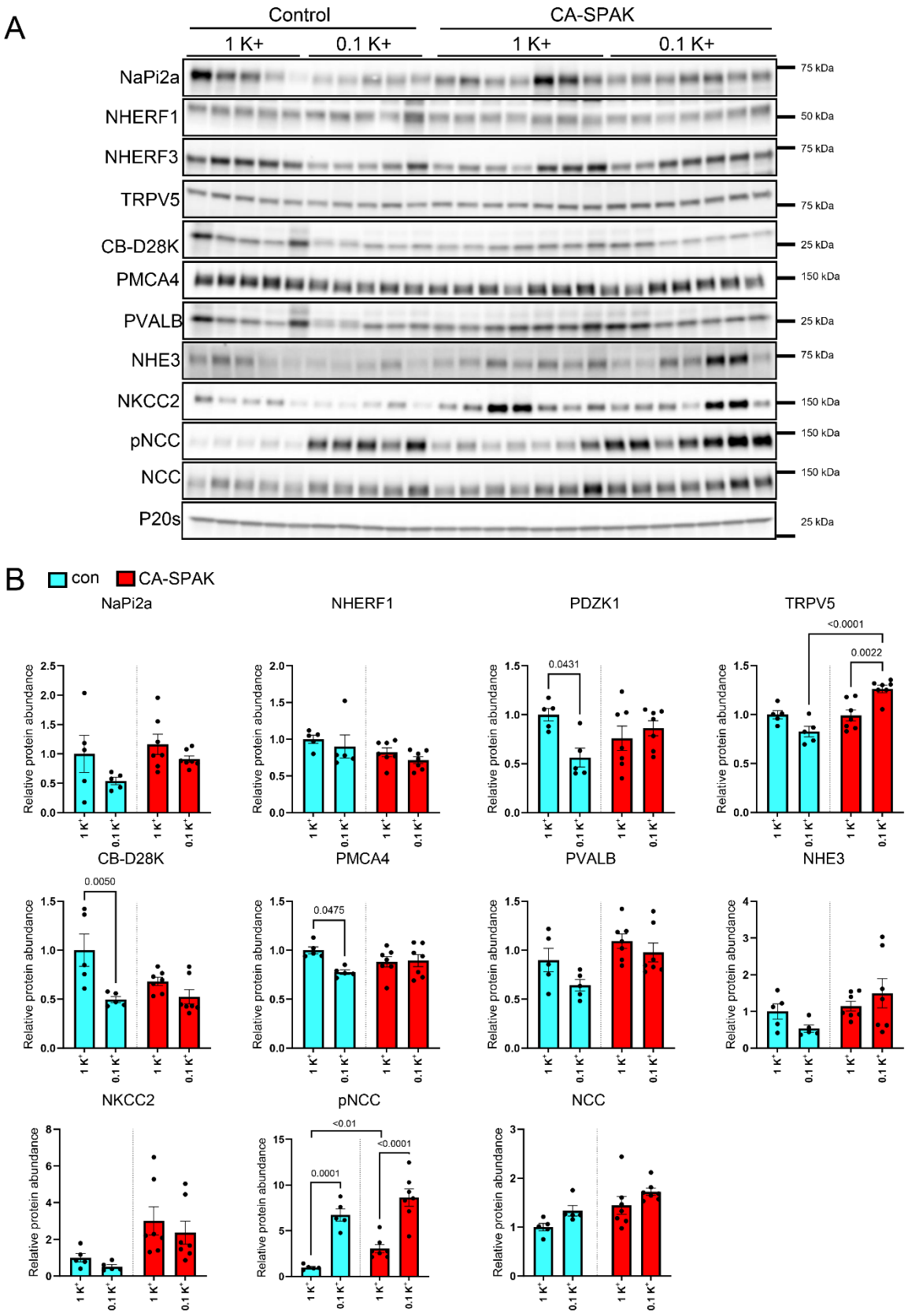
A
Control
CA-SPAK
1 K+
0.1 K+
1 K+
0.1 K+
NaPi2a
NHERF1
NHERF3
TRPV5
CB-D28K
PMCA4
PVALB
NHE3
NKCC2
pNCC
NCC
P20s
75 kDa
50 kDa
75 kDa
75 kDa
25 kDa
150 kDa
25 kDa
75 kDa
150 kDa
150 kDa
150 kDa
25 kDa
B
con
CA-SPAK
NaPi2a
NHERF1
PDZK1
TRPV5
<0.0001
0.0022
0.0431
CB-D28K
PMCA4
PVALB
NHE3
0.0050
0.0475
NKCC2
pNCC
NCC
<0.01
<0.0001
0.0001
Relative protein abundance